

RESEARCH ARTICLE

Control of Movement

## Confidence in predicted position error explains saccadic decisions during pursuit

Jonathan D. Coutinho,<sup>1</sup> Philippe Lefèvre,<sup>1,2,3</sup> and Gunnar Blohm<sup>1</sup>

<sup>1</sup>Centre for Neuroscience Studies, Queen's University, Kingston, Ontario, Canada; <sup>2</sup>Institute of Information and Communication Technologies, Electronics and Applied Mathematics, Université catholique de Louvain, Louvain-la-Neuve, Belgium; and <sup>3</sup>Institute of Neuroscience, Université catholique de Louvain, Louvain-la-Neuve, Belgium

### Abstract

A fundamental problem in motor control is the coordination of complementary movement types to achieve a common goal. As a common example, humans view moving objects through coordinated pursuit and saccadic eye movements. Pursuit is initiated and continuously controlled by retinal image velocity. During pursuit, eye position may lag behind the target. This can be compensated by the discrete execution of a catch-up saccade. The decision to trigger a saccade is influenced by both position and velocity errors, and the timing of saccades can be highly variable. The observed distributions of saccade frequency and trigger time remain poorly understood, and this decision process remains imprecisely quantified. Here, we propose a predictive, probabilistic model explaining the decision to trigger saccades during pursuit to foveate moving targets. In this model, expected position error and its associated uncertainty are predicted through Bayesian inference across noisy, delayed sensory observations (Kalman filtering). This probabilistic prediction is used to estimate the confidence that a saccade is needed (quantified through log-probability ratio), triggering a saccade upon accumulating to a fixed threshold. The model qualitatively explains behavioral observations on the frequency and trigger time distributions of saccades during pursuit over a range of target motion trajectories. Furthermore, this model makes novel predictions that saccade decisions are highly sensitive to uncertainty for small predicted position errors, but this influence diminishes as the magnitude of predicted position error increases. We suggest that this predictive, confidence-based decision-making strategy represents a fundamental principle for the probabilistic neural control of coordinated movements.

**NEW & NOTEWORTHY** This is the first stochastic dynamical systems model of pursuit-saccade coordination accounting for noise and delays in the sensorimotor system. The model uses Bayesian inference to predictively estimate visual motion, triggering saccades when confidence in predicted position error accumulates to a threshold. This model explains saccade frequency and trigger time distributions across target trajectories and makes novel predictions about the influence of sensory uncertainty in saccade decisions during pursuit.

*Bayesian; bounded accumulation; Kalman Filter; modeling; motor coordination*

### INTRODUCTION

The coordination between continuously controlled and discretely triggered movements to achieve a common goal remains a fundamental problem in neuroscience. This coordinated motor control is exemplified in the pursuit and saccadic eye movements that humans perform when tracking moving objects. Pursuit eye movements are continuously controlled to minimize the relative motion of a

visual image on the retina (1, 2). Due to noise and delays prevalent in sensorimotor systems (3, 4), pursuit trajectory may deviate from and lag behind the true target trajectory (5). Furthermore, eye velocity is typically lower than the target velocity (6, 7), resulting in an accumulation of position error during pursuit. As a result, the position of the visual image may drift outside the high acuity foveal region of the retina. Saccades are rapid eye movements that are discretely triggered to reposition the target



onto the fovea (8, 9). In addition to the categorization of continuous versus discrete movements as requiring versus omitting sensory feedback, respectively, a defining characteristic of discrete movements is their requirement for an externally timed trigger to initiate movement execution (10, 11). However, the decision process regulating the trigger of saccades during pursuit remains poorly understood. A quantitative model of this decision process has potential to illuminate key principles in the stochastic coordination of continuous and discrete movements for a common goal.

Previous studies have characterized the sensory conditions correlating with saccade trigger during pursuit, though these observations have not yet been synthesized into a mechanistic model. It has been well documented that pursuit can be initiated without executing saccades if the target is displaced backward (step) relative to its motion direction (ramp) such that it crosses the fixation position (target-crossing time,  $T_{XT}$ ) in  $\sim 200$  ms (12). This pattern of step-ramp target motion with target-crossing times slightly earlier or later than this critical 200-ms window tends to evoke saccade with long, variable latencies compared with targets whose motion is in the same direction as the step (13). A similar pattern of saccade frequency and trigger time distributions is observed during sustained, steady-state pursuit (14). Thus, the combination of position error and retinal slip are important signals influencing saccade trigger. In one dimensional, horizontal tracking, a documented behavioral correlate of saccade trigger is the negative ratio of position error to retinal slip (i.e., velocity error), which represents the time at which the eye trajectory will cross the target trajectory based on linear extrapolation (14). This ratio, originally named eye-crossing time ( $T_{XE}$ ), will henceforth be referred to as time-to-foveation (TTF) to parallel the nomenclature of time-to-collision and time-to-contact used in studies of steering and interception (15–17). Time-to-foveation correlates well with summary statistics of saccade frequency, but its ability to dynamically predict saccade decisions is limited when retinal slip is close to zero (time-to-foveation goes to infinity) or with two-dimensional target motion (where linear extrapolations of eye and target trajectory commonly fail to intersect). Thus, although existing data sets have outlined the influence of sensory signals on saccade frequency and trigger time, a quantitative model explaining trial-by-trial saccade decisions is still missing.

A framework commonly used in modeling decision-making under uncertainty is bounded evidence accumulation (18–22). In these models, noisy information is sequentially sampled and the likelihood that these data support a particular response is integrated over time. Responses are triggered when the accumulated evidence for that response reaches a threshold. Choices, response times, postdecision confidence, and neuronal responses in sensorimotor brain areas are consistent with this framework (23–29). Nevertheless, these stochastic decision models have had limited application in oculomotor control, since previous pursuit models relied on deterministic visual motion signals (30). However, recent Bayesian models successfully simulated the control of pursuit from noisy motion signals (31, 32), and predictions about

pursuit and saccadic amplitude programming have been validated (33). This provides a novel opportunity to model the stochastic, sensory basis of saccadic decision-making during pursuit.

Here, we propose a predictive, probabilistic decision mechanism for saccade trigger that explicitly accounts for sensorimotor delays and uncertainties. Retinal position, velocity, and acceleration errors are estimated from noisy, delayed sensory signals through Kalman filtering and predictively extrapolated to overcome sensorimotor delays. Saccades are triggered when saccade confidence accumulates to a threshold. We define saccade confidence as the log probability ratio of the predicted position error being outside the foveal center. This definition has roots in the sequential probability ratio test (34, 35) and agrees with the proposition that the term confidence should reflect the probability that a response/action is appropriate given the observed evidence (36). Furthermore, this framework has a plausible neural basis in probabilistic population coding (37–40). The model simulates saccade frequency and trigger time distributions evoked by a wide range of step-ramp target motion trajectories and makes novel predictions about the influence of increased sensory uncertainty (e.g., by blurring the visual target or due to signal-dependent noise). The model illustrates how predictive probabilistic decision-making can flexibly coordinate continuously controlled and discretely triggered orienting movements for a common goal. We suggest this stochastic, predictive, confidence-based decision mechanism represents a fundamental principle in the neural control of motor coordination.

## METHODS

### Model Overview

The purpose of this model is to explain the sensory basis of saccadic decision-making during smooth pursuit eye movements. Using a recent Bayesian model of motion estimation and pursuit dynamics (32), we develop a novel stochastic evidence accumulation model of saccade triggering. The overall model consists of three interconnected modules: a sensory pathway for predictive state estimation, a decision pathway for evidence accumulation, and a motor pathway implementing the dynamics of eye motion (Fig. 1). The key features of the sensory pathway are recursive Bayesian inference for state estimation (Fig. 1, Kalman filtering) and prediction through linear motion extrapolation (Fig. 1, sensory extrapolation) to compensate for sensorimotor delays and predict future position error. The decision mechanism uses a predictive, probabilistic position error estimate to compute the log-probability ratio that the target is left versus right of the fovea (which we define as saccade confidence). A saccade is triggered when leaky accumulation of saccade confidence reaches a threshold value. We use this model to simulate trial-by-trial visual tracking and predict frequency and trigger time distributions of saccades evoked by a range of step-ramp target motion trajectories.

We will denote matrices and vectors in bold and scalars in unbolded case. Symbols with hat (^) denote estimates of latent variables.

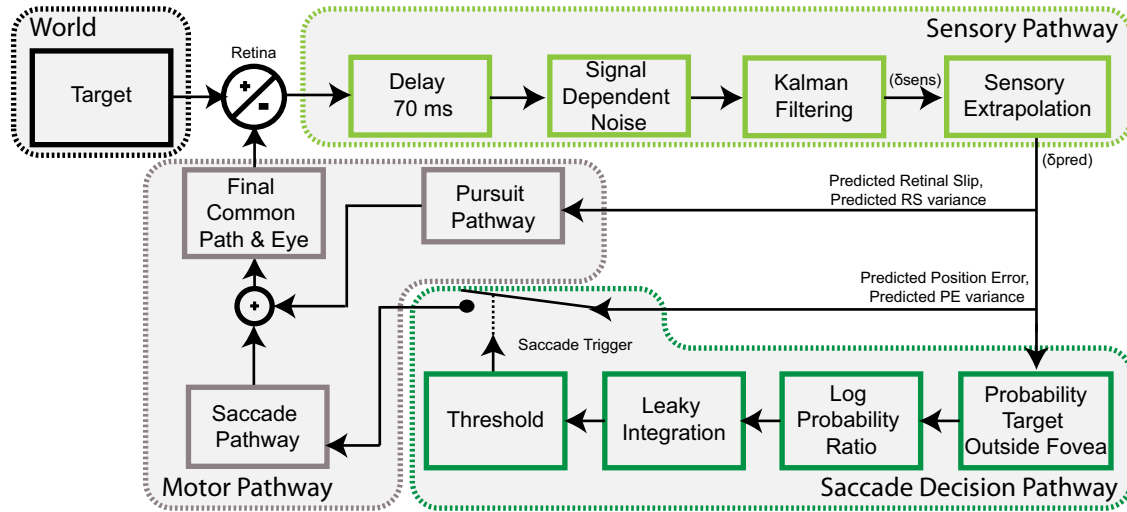


**Figure 1.** Global overview of model architecture. Sensory pathway (light green): retinal state information is delayed, corrupted by signal-dependent noise, then estimated through Kalman filtering, and predictively extrapolated to generate predicted position error and predicted retinal slip. Saccade decision pathway (dark green): predicted position error and its associated uncertainty are used to compute the log-probability ratio that the target is left vs. right of the fovea. This value, defined as saccade confidence, is accumulated by a leaky integrator to trigger saccades upon threshold crossing. Motor pathway (gray): describes the premotor commands for saccades and pursuit, which are linearly combined in the final common pathway (eye plant) implementing the dynamics of eye motion. PE, position error; RS, retinal slip;  $\delta^{sens}$ , sensory retinal state;  $\delta^{pred}$ , predicted retinal state.

## Sensory Pathway

The sensory pathway is founded on the visual motion processing pathway previously described (32). The true (deterministic) retinal state,  $\delta^{det}$ , is defined as the difference between the position, velocity, and acceleration of the target,  $\mathbf{t}$ , and the eye,  $\mathbf{e}$ :

$$\delta_k^{det} = \mathbf{t}_k - \mathbf{e}_k = \begin{bmatrix} PE_k^{det} \\ RS_k^{det} \\ RA_k^{det} \end{bmatrix} \quad (1)$$

where  $PE_k^{det}$  is position error,  $RS_k^{det}$  is retinal slip,  $RA_k^{det}$  is retinal acceleration, and  $k$  represents the current discrete time step in the numerical simulation (1-ms time steps).

The observed retinal state,  $\delta^{obs}$ , is delayed by 70 ms (30, 41) and corrupted by additive and signal-dependent noise:

$$\delta_k^{obs} = \delta_{k-70}^{det} + \Phi_{mult} \delta_{k-70}^{det} + \phi_{add} \quad (2)$$

where  $\Phi_{mult}$  and  $\phi_{add}$  are uncorrelated noise covariance matrices with values drawn from  $\phi_{mult} \sim N(0, \sigma_{mult}^2)$  and  $\phi_{add} \sim N(0, \sigma_{add}^2)$  at each time step. The values of noise parameters are listed in Table 1. These terms represent the signal-dependent and baseline noise levels corrupting visual sensory information. Both behavioral and electrophysiological data are consistent with this noise structure in the position and motion information driving saccades and pursuit (5, 42–47).

Using delayed, noisy observations of image motion, a Bayes-optimal probabilistic estimate of retinal state,  $\hat{\delta}^{sens}$ , is computed through Kalman filtering (32, 48). This method of recursive Bayesian estimation combines noisy observations ( $\delta^{obs}$ ) with priors of the noise characteristics and dynamics of the world (i.e., a generative model) to estimate retinal state. This generative model assumes the

evolution of retinal state can be described by an uncorrelated random walk:

$$\delta_{k+1}^{sens} = \delta_k^{sens} + \lambda_k \quad (3)$$

where  $\lambda$  is an uncorrelated additive noise with  $\lambda \sim N(0, \mathbf{Q}^2)$  representing the state variability, a prior belief about how retinal state changes over time. The generative model also contains priors about the noise characteristics of visual observations of retinal state:

$$\delta_k^{obs} = \mathbf{Y}_k \delta_{k-70}^{sens} + \mathbf{v}_k \quad (4)$$

where  $\mathbf{Y}$  and  $\mathbf{v}$  are the expected, uncorrelated signal-dependent and additive noise covariance matrices with  $\mathbf{Y} \sim N(0, \mathbf{D}^2)$  and  $\mathbf{v} \sim N(0, \mathbf{R}^2)$ . These terms represent the brain's learned estimates of the noise characteristics of sensory observations. We set  $\mathbf{D}^2 = \sigma_{mult}^2$  and  $\mathbf{R}^2 = \sigma_{add}^2$ . This corresponds to an accurate estimate of noise parameters, although it has been shown an exact knowledge of these values is not crucial (32, 49).

Kalman filtering combines the current estimate of retinal state,  $\hat{\delta}_k^{sens}$ , the current noisy observation,  $\delta_k^{obs}$ , and prior knowledge of noise characteristics,  $\mathbf{R}$ ,  $\mathbf{D}$ , and  $\mathbf{Q}$ , to optimally estimate retinal state at the next time step (50, 51):

$$\hat{\delta}_{k+1}^{sens} = \hat{\delta}_k^{sens} + \mathbf{K}_k (\delta_k^{obs} - \hat{\delta}_k^{sens}) + \eta_k \quad (5)$$

$$\mathbf{K}_k = \Sigma_k^{sens} \left( \Sigma_k^{sens} + \mathbf{R}^2 + \mathbf{D}^2 \left( \Sigma_k^{sens} + \hat{\delta}_k^{sens} \hat{\delta}_k^{sensT} \right) \mathbf{D}^{2T} \right)^{-1} \quad (6)$$

$$\Sigma_{k+1}^{sens} = \mathbf{Q}^2 + \mathbf{\Omega}^2 + (\mathbf{I} - \mathbf{K}_k) \Sigma_k^{sens} \quad (7)$$

where  $\Sigma^{sens}$  is the estimated error covariance of the retinal state estimate,  $\mathbf{K}$  is the Kalman gain, and  $\mathbf{I}$  is the identity matrix. The Kalman gain is calculated and used to weigh incoming sensory evidence according to its relative reliability

**Table 1.** Values of noise parameters used in sensory pathway Kalman filtering for retinal position, velocity, and acceleration

Parameter Name	Parameter Symbol	Parameter Value
Additive sensory noise variance	$R^2$	$\begin{bmatrix} 0.25^2 \\ 7.5^2 \\ 50^2 \end{bmatrix}$
Signal-dependent sensory noise covariance	$D^2$	$\begin{bmatrix} 1 & 0 & 0 \\ 0 & 1.5^2 & 0 \\ 0 & 0 & 1 \end{bmatrix}$
Estimated state variability	$Q^2$	$\begin{bmatrix} 0.1 \\ 1 \\ 30 \end{bmatrix}$
Internal sensory process noise	$\Omega^2$	$\begin{bmatrix} 0.1 \\ 0.3 \\ 10 \end{bmatrix}$

compared with the current optimal estimate.  $\eta$  is the internal noise of estimation with  $\eta \sim N(0, \Omega^2)$ , which represents variability in the estimation process. The values of Kalman filtering parameters are listed in Table 1.

In the final, predictive stage of the sensory pathway, retinal state is linearly extrapolated through prior knowledge of sensorimotor delays. It has been shown that saccades can accurately foveate moving targets, requiring motion-based prediction to extrapolate saccade amplitudes to compensate for the visuomotor delay and ensuing target displacement during saccade execution (52–56). Similarly, it has been shown that motion information driving pursuit accounts for both velocity and acceleration, which minimizes instability in pursuit dynamics (57–59). Our model hypothesizes that the same predictive position error signal for programming saccade amplitude is used in the mechanism deciding saccade trigger:

$$\hat{\delta}_k^{pred} = \begin{bmatrix} \widehat{PE}_k^{pred} \\ \widehat{RS}_k^{pred} \end{bmatrix} = \begin{bmatrix} 1 & T_{sacc} & 0 \\ 0 & 1 & T_{purs} \end{bmatrix} \hat{\delta}_k^{sens} \quad (8)$$

$$\Sigma_k^{pred} = \begin{bmatrix} \Sigma_k^{PEpred} \\ \Sigma_k^{RSpred} \end{bmatrix} = \begin{bmatrix} 1 & (T_{sacc})^2 & 0 \\ 0 & 1 & (T_{purs})^2 \end{bmatrix} \Sigma_k^{sens} \quad (9)$$

where  $T_{sacc} = 125$  ms and  $T_{purs} = 70$  ms represent the time constant of extrapolation for each respective signal. The rationale for the longer extrapolation time for position error is to account for the additional decision accumulation time, motor delay, and movement duration specific to the saccadic movement system (60).

### Saccade Decision Pathway

The saccade decision pathway is inspired by the sequential probability ratio test and stochastic bounded accumulation models of decision-making (26, 35). This pathway computes the evidence that the target is outside the fovea,

i.e., the log-probability ratio of the target being left ( $P^{Left}$ ) versus right ( $P^{Right}$ ) of the fovea:

$$P_k^{Left} = 1 - P_k^{Right} = cdf\left(\widehat{PE}_k^{pred}, \Sigma_k^{PEpred}\right) \quad (10)$$

$$= \int_{-\infty}^0 \frac{1}{\sqrt{2\pi\Sigma_k^{PEpred}}} \exp\left(-\frac{(x - \widehat{PE}_k^{pred})^2}{2\Sigma_k^{PEpred}}\right) dx$$

where  $cdf(mean, variance)$  represents the cumulative distribution function of a Gaussian distribution (i.e., predicted position error) evaluated at zero (i.e., the fovea).

Saccade confidence ( $\hat{C}$ ) is updated through leaky integration of this evidence:

$$current\ evidence = \log\left(\frac{P_k^{Right}}{P_k^{Left}}\right) \quad (11)$$

$$\hat{C}_k^{Right} = -\hat{C}_k^{Left} = \hat{C}_{k-1}^{Right} + \left(\frac{dt}{\tau_s}\right) (current\ evidence - \hat{C}_{k-1}^{Right}) \quad (12)$$

where  $\tau_s = 25$  ms is the time constant of leaky integration. When predicted PE is close to zero,  $P^{Right}$  and  $P^{Left}$  are close in value ( $\sim 0.5$ ), and thus saccade confidence is close to zero ( $\log(1) = 0$ ). When predicted PE is small, saccade confidence decreases as  $\Sigma_k^{PEpred}$  increases. When predicted PE is large, saccade confidence is less sensitive to  $\Sigma_k^{PEpred}$ . This stems from the cumulative distribution function (evaluated at zero) changing nonlinearly with mean and variance. Using leaky integration (Eq. 12), the weight of past evidence exponentially decays at a rate specified by  $\tau_s$ , biasing decision-making toward recent evidence and preventing instantaneous confidence outliers to erroneously trigger a saccade. The estimate of saccade confidence ( $\hat{C}$ ) acts as a decision variable triggering saccades when its magnitude exceeds  $\theta_{saccade} = 4.0$ . This value corresponds to a 98.2% probability that the target is displaced from the center of the fovea in a specific horizontal direction. These values of  $\tau_s$  and  $\theta_{saccade}$  were selected by manually tuning parameters to generally match the qualitative trends in saccade frequency and trigger time observed in previously reported step-ramp tracking experiments. The effects of varying these parameter values on saccade frequency and trigger time is illustrated in Fig. 13. Crucially, using experimental data from (61), we calculated optimally fit parameter values individually for our participants to validate our parameter value choices in describing human saccade-pursuit coordination (described in Model Fitting).

A simplified model of saccade dynamics and refractory period were implemented from (62) (see Saccade Motor Pathway below) to illustrate how this decision model can be incorporated into a global framework of oculomotor control.

### Pursuit Motor Pathway

The pursuit motor pathway transforms the predicted retinal slip,  $\widehat{RS}^{pred}$ , into an oculomotor command that is sent to the premotor system and eye plant. It is adapted from the image velocity motion pathway and positive efferent copy feedback loop used by previous models (30, 32, 63). The pathway (Fig. 2,

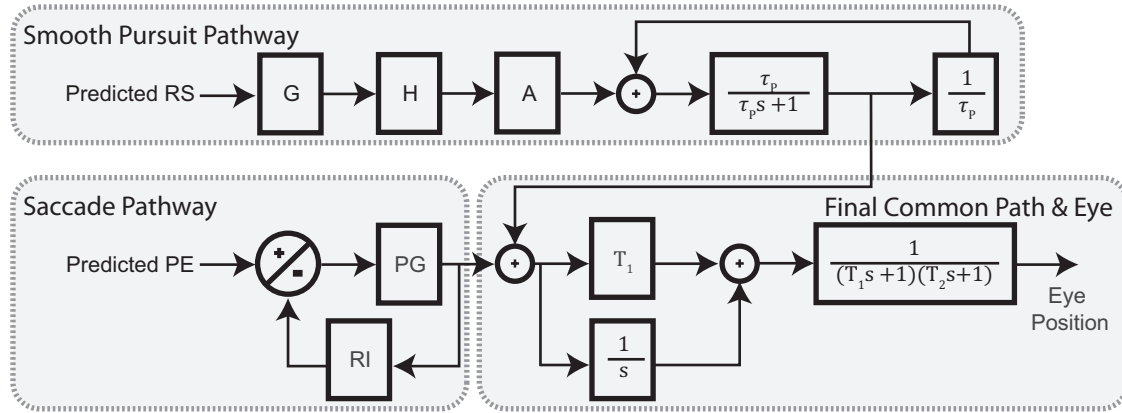


**Figure 2.** Overview of motor pathway. Pursuit motor commands are continuously generated from predicted retinal slip, whereas saccade motor commands are generated from predicted position error when saccade confidence reaches threshold. Pursuit and saccade motor commands are linearly combined in the final common pathway, representing the neural integration of oculomotor commands for maintaining gaze position and the neuromuscular dynamics of eye motion. In the pursuit pathway,  $G$  is a nonlinear function,  $H$  is a second order filter,  $A$  is a linear gain,  $\tau_p$  is a time constant for leaky-integrated positive feedback. In the saccade pathway,  $PG$  stands for pulse generator,  $RI$  stands for resettable integrator (which tracks the progress of each saccade and is reset at saccade offset). In the final common pathway,  $T_1$  and  $T_2$  are time constants describing the dynamics of eye motion and parameters of the final neural integrator.

Pursuit Motor Pathway, *Eqs. 13–15*) contains a nonlinear transfer function ( $G$ ) to convert the RS input into an oculomotor command, a second-order filter ( $H$ ) to adjust the time course of inputs, and a variable gain element ( $A$ ). The parameters were taken from Krauzlis and Lisberger, 1994 (30, 32, 58).

$$G(\widehat{RS}^{pred}) = 7\widehat{RS}^{pred} \quad (13)$$

$$H(s) = \frac{35^2}{s^2 + (2)(0.8)(35)s + 35^2} \quad (14)$$

$$A = 0.9 + \zeta_{trial} \quad (15)$$

where  $s$  represents the Laplace variable, and  $\zeta_{trial} \sim N(0, \sigma_{purs}^2)$ , with  $\sigma_{purs}^2 = 0.05$ . The purpose of this noise term in *Eq. 15* is to simulate the trial-by-trial variability in pursuit gain observed in human behavioural responses, thus capturing a realistic level of pursuit variability and consequent trial-by-trial variability in sensory signals based on pursuit performance (64, 65). Although sensory uncertainty is a major source of pursuit variability (5), behavioral evidence suggests further motor-related variability influencing pursuit gain that can be dissociated from motion perception (66, 67).

The output of this image velocity motion pathway is sent to a leaky integrator with positive feedback, maintaining eye velocity when  $\widehat{RS}_k^{pred} = 0$ . The leaky integrator is characterized by a single time constant,  $\tau_p = 100$  ms. The positive feedback loop contains a linear gain element,  $\frac{1}{\tau_p}$ , balancing the strength of positive feedback versus leak (30, 32).

### Saccade Motor Pathway

After saccade confidence reaches the decision threshold, the saccade motor pathway (*Fig. 2*, Saccade Pathway) transforms a desired saccade amplitude into an oculomotor command that is sent to the premotor system and eye plant. It has been shown that saccade amplitude is programmed by the predicted position error,  $\widehat{PE}^{pred}$ , at trigger time (68, 69).

The purpose of this saccade model was not to exactly reproduce all aspects of saccade dynamics, but rather to embed a simple, illustrative model of saccade execution within our global framework of oculomotor control. A motor delay of 40 ms was implemented between the time of saccade confidence threshold crossing and the execution of the saccade. The model of saccade dynamics is adapted from the local feedback model and bilateral burst neuron discharge rate pulse generator (*Fig. 2*,  $PG$ ) used by Blohm et al. (62), Jürgens et al. (70), and Scudder (71). In this pathway, the desired saccade amplitude is compared against an internal estimate of executed eye movement through negative feedback from a resettable integrator (*Fig. 2*,  $RI$ ), providing an estimate of ongoing motor error without requiring visual feedback. This motor error is sent to a pulse generator, providing a saccadic motor command sent to the premotor system and eye plant. The pulse generator was based on the bilateral burst neuron discharge rate proposed by Van Gisbergen et al. (72):

$$y = \begin{cases} -b_m(1 - e^{-\frac{x-e_0}{b_k}}) & \text{if } x < e_0 \\ b_m(e^{\frac{x-e_0}{b_k}} - e^{-\frac{x-e_0}{b_k}}) & \text{if } -e_0 < x < e_0 \\ b_m(1 - e^{-\frac{x-e_0}{b_k}}) & \text{if } x > e_0 \end{cases} \quad (16)$$

where the input,  $x$ , is the motor error and the output,  $y$ , is a saccadic motor command approximating the main sequence relationship between saccade amplitude, peak velocity, and duration (73). The parameters used match (62) (i.e.,  $e_0 = 1$  deg;  $b_m = 600$  deg/s; and  $b_k = 3$  deg). Note, that we used an oversimplified saccade generator since saccades were only produced for illustrative purposes and did not affect the smooth pursuit or decision mechanisms. Also, we were only interested in the temporal evolution of trials up until saccade trigger; we thus omitted any variability terms in saccade amplitude that would be required for more realistic catch-up saccade behavior. Furthermore, we avoid speculating on the problem of how retinal signals during the saccade are

processed (but see Ref. 74) and how they may influence subsequent pursuit (75, 76).

### Final Common Motor Pathway and Eye Plant

Oculomotor commands from the pursuit and saccade pathways are linearly added then sent through the premotor system to the eye plant. The premotor system consists of the sum of the motor command (with gain =  $T_1 = 170$  ms) and its integral, producing the pulse-step innervation pattern required to displace the eye and maintain eccentricity (77). This gain term ensures an appropriate weighting between the proportional and integral components. The eye plant is modeled as an overdamped, second-order system with time constants  $T_1 = 170$  ms and  $T_2 = 13$  ms. No additional motor noise was added to the eye plant, as the moment-by-moment variability in sensory observations and trial-by-trial variability in pursuit gain that we implemented provides a sufficiently realistic distribution of motor variability (5, 78, 79).

### Simulations

The model was numerically simulated in MATLAB R2018b (MathWorks, Natick, MA) using 1-ms discrete time steps. We simulated eye movements in response to horizontal step-ramp target motions selected to reproduce behavioral experiments of pursuit initiation (Figs. 4 and 5; compare to Ref. 13) and pursuit maintenance (Figs. 6, 7, and 8; compare to Ref. 14). For pursuit initiation, we simulated target position steps (PS) between 1 to 12 degrees in one-degree increments, target velocity steps (VS) of  $\pm 10$  deg/s and  $\pm 20$  deg/s (where positive values represent right and negative values represent left), and 100 repetitions at each step-ramp condition. For pursuit maintenance, the initial step-ramp was selected to recross the initial fixation position in 200 ms, thus minimizing initial saccade frequency. The step sizes used were 2, 4, and 6 degrees with velocity changes of 10, 20, and 30 deg/s, respectively, in the opposite direction. The second step-ramp was selected using velocity steps of  $\pm 10$ , 20, and 40 deg/s with corresponding position steps such to provide a range of target crossing times between  $-300$  ms to 700 ms in 20-ms increments ( $T_{XT} = -PS/VS$ ), with 50 repetitions per double step-ramp condition. Using our model, we simulated single trials of eye movement responses and calculated saccade trigger time (defined as the duration between saccade onset and the previous change in target motion) for trials containing saccades. The simulated distributions of saccade frequency and trigger time as a function of target parameters were compared with experimental data. The target parameters for the pursuit maintenance study were also selected because they test different combinations of (PS, VS) that correspond to an equal target crossing time and similar time-to-foveation values following the change in target motion. This allowed us to compare our model against the time-to-foveation model (which predicts no differences in behavioral responses for combinations of PS, VS with identical TTF). TTF was calculated at trigger time in trials with at least one saccade, or in smooth trials by taking the time average across the first 400 ms following step-ramp onset. Trigger time corresponded to the saccade latency with respect to PS/VS occurrence and was computed using a  $500 \text{ deg/s}^2$  acceleration threshold (60) to match experimental data analysis.

To test the influence of sensory uncertainty on saccade behavior, we repeated simulations using the same double step-ramp target motion conditions while modifying the variance of the additive and multiplicative noise in position estimation to  $2^2 \text{ deg}^2$  and  $1.5^2$ , respectively (Fig. 10). We analyzed the proportion of trials with at least one saccade and the trigger time of the first occurring saccade after each step-ramp.

We tested the effects of decision parameter variation on saccade frequency and trigger time (Fig. 11), by simulating visual tracking to a  $-20 \text{ deg/s}$  step-ramp target with varying position steps from  $-4$  to 10 degrees (100 repetitions per step-ramp condition) while varying a single decision parameter (leaving the rest at the values originally described). Decision accumulator leaky integration time constant ( $\tau_s$ , Eq. 12) was varied between 10 to 75 ms, saccade confidence decision threshold ( $\theta_{saccade}$ ) was varied between 3.5 and 4.5, or sensory position extrapolation duration varied from 50 to 250 ms ( $T_{sacc}$ , Eq. 8). The code for the full model and all simulations is available on GitHub (<https://github.com/BlohmLab/SaccadeTriggerModel>).

### Model Fitting

The goal of model fitting was to use empirical data from humans performing visual tracking of step-ramp target trajectories (61) to evaluate our choices in parameter values in our model and quantify the range of parameter values that can be expected given variability of behavior across participants. Specifically, the goal was not to use our model to make quantitative characterizations of individual participants, but rather to use participant-by-participant data to evaluate whether our choices in model parameters were realistic. We implemented fitting using maximum-likelihood estimation and the Bayesian Adaptive Direct Search (BADS) toolkit (80) to estimate optimal parameters directly pertaining to the trigger mechanism ( $T_{sacc}$ ,  $\tau_s$ ,  $\theta_{saccade}$ ) for each participant (i.e., sensory motion extrapolation time, saccade decision pathway leaky accumulation time constant, saccade trigger threshold) while keep all other parameters unchanged. To do so, for each single trial of experimental data, we used the time-varying values of position error and retinal slip from the eye tracker as inputs to the model ( $PE^{det}$ ,  $RS^{det}$ ) (Eq. 1). We then simulated the sensory pathway (Eqs. 2–9) and saccade decision pathways (Eqs. 10–12) but did not simulate any motor pathways; thus, the input to the model was entirely based on the participants' actual eye motion with respect to the tracking target, not simulated eye movements (thus eliminating potential bias from mismatch between simulated pursuit and human behavior). We calculated the simulated trigger time and repeated this process (with the same PE, RS input) 1,000 times to evaluate an empirical probability density function for saccade trigger time given a single particular trial of experimental data. Using the empirical trigger time in this trial, we calculated the likelihood of this data point given the empirical (simulated) trigger time probability distribution. We summed the likelihoods across all trials for a single participant to obtain the overall likelihood of the data given the model parameters, and used BADS to iteratively discover the optimal parameter values to maximize the overall likelihood across all trials.

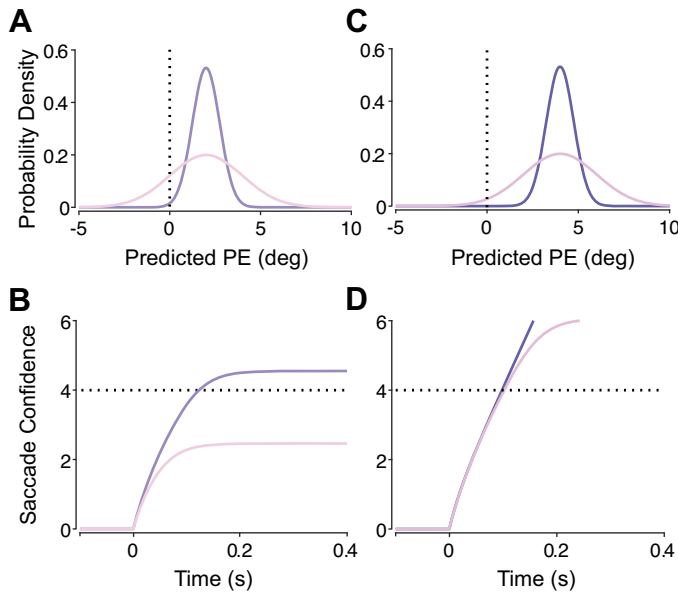


**Figure 3.** Schematic diagram of the temporal evolution of saccade confidence from constant, probabilistic predicted PE estimates. **A:** small predicted PE (2 deg) with high (pink) and low (purple) uncertainty. **B:** this results in small (pink) and large (purple) saccade confidence values. **C:** large predicted PE (4 deg) with high (pink) and low (purple) uncertainty. **D:** this results in little difference in saccade confidence and highly similar decision trigger time. In **B** and **D**, the horizontal dotted line represents the threshold to trigger a saccade. PE, position error.

## RESULTS

This model of oculomotor control relies on Bayesian estimation of stochastic sensory signals and bounded evidence accumulation to trigger saccades upon threshold crossing. The notable novelty of this model is the computation of saccade confidence from a probabilistic prediction of position error. We define saccade confidence as the log-probability ratio that the image is left versus right of the fovea center. Saccades are triggered when confidence is leaky accumulated to a threshold value.

### Computation of Saccade Confidence

Saccade confidence is computed from the log-probability ratio of the target being left versus right of the fovea (Eqs. 10 and 11) and leaky integrated over time (Eq. 12). This process is schematically shown in Fig. 3, where a constant predicted PE input is used to illustrate the evolution of saccade confidence over time (although in the normal operation of this model, predicted PE and its uncertainty are time varying based on noisy and evolving retinal state observations). Figure 3A illustrates the probability density function for a predicted PE of 2 degrees with low uncertainty (purple) and high uncertainty (pink). The probability of the target being right of the fovea,  $P^{Right}$ , is the area under the probability density to the right of zero (denoted in vertical dashed line). The natural logarithm of the ratio between  $P^{Right}$  and  $P^{Left}$  is leaky integrated to compute saccade confidence, whose temporal evolution is illustrated in Fig. 3B. With low magnitude PE, the temporal evolution of saccade confidence is highly sensitive to uncertainty, and in the case of an unreliable target, even no saccade would be triggered. Figure 3C illustrates

a predicted PE of 4 degrees, with low uncertainty (purple) and high uncertainty (pink). Figure 3D shows the time evolution of saccade confidence for this PE input, whose time course is much less sensitive to uncertainty because of the larger magnitude PE. This is from the nonlinearity in the cumulative distribution function evaluated at zero with changes in mean and variance. Thus, the estimation of saccade confidence accounts for both predicted PE and its uncertainty, but this computation is more sensitive to uncertainty for targets closer to the fovea.

### Decision Process during Pursuit Initiation

To illustrate how sensory signals influence saccadic decision making, Fig. 4 plots single-trial simulations of oculomotor responses during pursuit initiation to two different step-ramp trajectories known to evoke high (red trace) and low (blue trace) saccade frequency, as well as a static step of target position (gray trace). The step-ramp trajectories contain an abrupt, simultaneous position displacement and constant velocity shift. This paradigm is commonly used to investigate saccadic decision-making during pursuit because it allows the experimenter to precisely control retinal state subsequent to the step-ramp onset (12–14, 60, 81).

In our model, retinal state is estimated from noisy and delayed sensory observations through Kalman filtering (Fig. 4, B and C) and predictively updated through linear extrapolation (Fig. 4D). This predicted PE is used to compute saccade confidence, which is leaky integrated to trigger saccades upon threshold crossing (horizontal dashed lines in Fig. 4E). In Kalman filtering, noisier signals (e.g., RS compared with PE) require more time for accurate estimation, which is comparable with data suggesting a late, asynchronous influence of RS compared with PE in saccade programming (82). The observation that saccade latency is longer than pursuit latency is explained by the additional temporal accumulator in the saccade decision pathway, intentionally procrastinating decision-making to allow for more accurate RS information to accrue and influence the decision. Thus, RS can either enhance or attenuate the evolution of saccade confidence by updating PE away from or toward the fovea, influencing the frequency and trigger time of saccades.

To reproduce previous findings (13), we simulated oculomotor responses across a range of step-ramp target trajectories and calculated the proportion of trials with at least one saccade and mean saccade trigger time. Figure 5 plots saccade proportion (Fig. 5, A and C) and mean saccade trigger time (Fig. 5, B and D) for a variety of step-ramp trajectories where the target velocity either moved toward the fovea (foveopetal) or away from the fovea (foveofugal). This model captures the major trends in behavioral data, replicating the minimization of saccade frequency when target-crossing time ( $-PS/V_S$ ) is near 200 ms (referred to as the smooth zone) (12), which is the case for a 4-deg step with a target moving at  $-20$  deg/s as in Fig. 5A, or a 2-deg step with the target moving at  $-10$  deg/s as in Fig. 5C (foveopetal condition). Furthermore, the model replicates the finding of long saccade trigger time for targets with target-crossing times slightly shorter or longer than the 200-ms smooth zone (compare with Fig. 2 in 13). Overall, the model reproduces the known trends in saccade trigger during pursuit initiation.

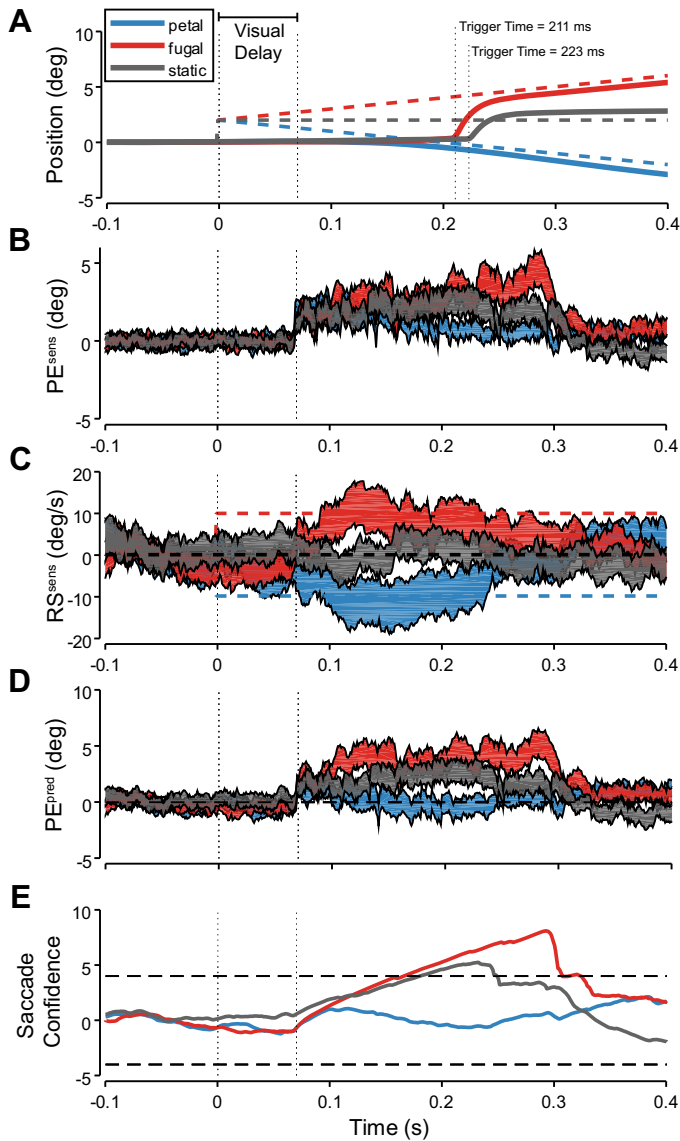


**Figure 4.** Single trial simulations of pursuit initiation. *A*: eye (solid, colored) and target (dashed, colored) position over time for a static position step in target (gray) and two step-ramp targets known to evoke high (red) and low (blue) saccade frequency. *B*: sensory position error over time, estimated from Kalman filtering. Patches represent the estimated value  $\pm$  its associated uncertainty (SD). *C*: sensory retinal slip over time, estimated from Kalman filtering. *D*: predicted position error over time, estimated by linearly extrapolating sensory position error according to retinal slip. *E*: saccade confidence over time, estimated from leaky integrating the log-probability ratio of the target being outside the fovea. Horizontal dashed lines indicate decision threshold. PE, position error; pred, predictive estimate; RS, retinal slip; sens, sensory estimate.

### Decision Process during Sustained Pursuit

The model was also developed to capture saccade decision-making during sustained pursuit using target trajectories with an initial Rashbass paradigm to minimize initial saccades, followed by a second step-ramp during steady state tracking (double step-ramp paradigm) (14). Figure 6 illustrates single-trial simulations, contrasting smooth and saccadic pursuit in response to a foveopetal and foveofugal step-ramp target perturbation during sustained pursuit.

Consistent with saccadic decisions during pursuit initiation, RS estimates that reduce predicted PE (due to RS and PE in opposite directions) result in reduced saccade confidence and subsequent absence of saccade trigger.

Across a range of double step-ramp target trajectories, we found that the sensory conditions preceding saccade trigger in simulations were highly comparable with human behavioral data. Figure 7 illustrates the sensory (Fig. 7A) and true (Fig. 7B) values of RS and PE preceding each saccade. The region of this phase plot delimited by solid lines is referred to by de Brouwer and colleagues (14) as the smooth zone. The slopes of these lines correspond to single time-to-foveation values. This demonstrates that the model replicates similar correlations between time-to-foveation and human saccade behavior, namely, that saccades are minimized when time-to-foveation is between 40 and 180 ms (the slopes of the lines plotted in Fig. 7). Thus, the smooth zone as described by de Brouwer et al. (60) reflects the range of target motion parameters that lead to small predicted position error and low probability of saccade trigger. Furthermore, the model simulated saccades with unusually long trigger time occurring when time-to-foveation (TTF) was slightly outside this range (Fig. 7, black dots; Fig. 9B). Thus, the model also explains saccadic decisions during sustained pursuit.

To further evaluate the relationship between this proposed saccade decision mechanism and previous correlations

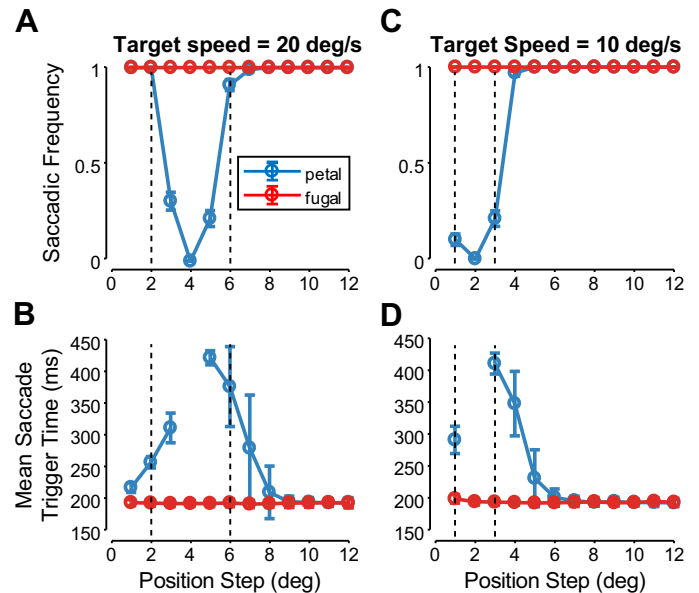


**Figure 5.** Summary statistics of simulated saccade decisions evoked by step-ramp target motion with position and velocity steps in the same direction (foveofugal, red) or opposite directions (foveopetal, blue), replicating the main findings of 13 (see their Fig. 2). For each step-ramp condition, 100 trial repetitions were simulated using a target speed of 20 deg/s and 10 deg/s, respectively. Vertical dashed lines indicate  $T_{XT} = 100$  ms and  $T_{XT} = 300$  ms (approximately marking the limits of the smooth zone in the Rashbass paradigm). *A* and *C*: proportion of trials evoking saccades in the first 450 ms is plotted against position step size using a target velocity of +20 deg/s (*A*) and +10 deg/s (*C*) (red, foveofugal) or -20 deg/s (*A*) and -10 deg/s (*C*) (blue, foveopetal). *B* and *D*: mean saccade trigger time  $\pm$  SD is plotted against position step size using a target velocity of +20 deg/s (red) and -20 deg/s (blue) (*B*) or using a target velocity of +10 deg/s (red) and -10 deg/s (blue) (*D*).  $T_{XT}$ , target-crossing time.

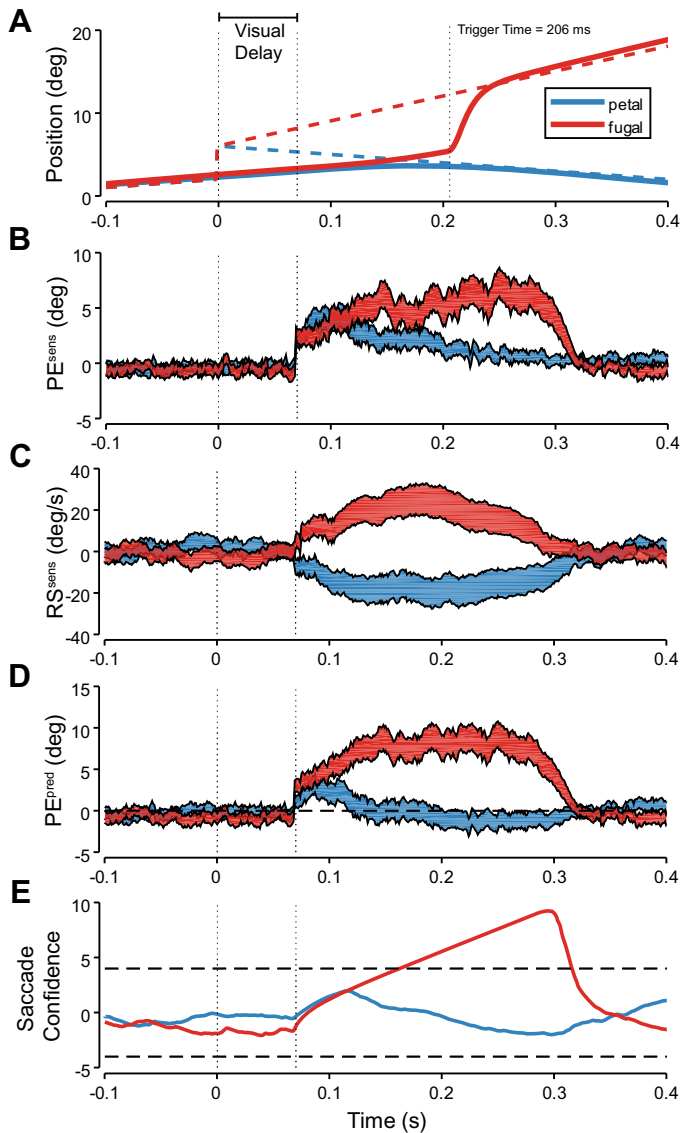


**Figure 6.** Single trial simulations of step-ramp perturbations in target motion during steady-state pursuit. Using a Rashbass step-ramp (step =  $-2$  deg, velocity =  $10$  deg/s) to smoothly initiate pursuit (Time  $< 0$  s, not shown), a second step-ramp target perturbation (Time =  $0$  s) with step =  $4$  deg, velocity =  $+20$  deg/s (red, foveofugal) or velocity =  $-20$  deg/s (blue, foveopetal). *A*: eye and target position over time. *B*: sensory position error over time, estimated through Kalman filtering. Patches represent the estimated value  $\pm$  its associated uncertainty (SD). *C*: sensory retinal slip over time, estimated through Kalman filtering. *D*: predicted position error over time, estimated through sensory extrapolation. *E*: saccade confidence over time, estimated through leaky-integrated log-probability ratio. PE, position error; pred, predictive estimate; RS, retinal slip; sens, sensory estimate.

between saccade trigger and time-to-foveation, we compared the evolution of position error and retinal slip during pursuit with their resulting saccade confidence values. Figure 8 illustrates average saccade confidence contours as a function of position error and retinal slip, along with the evolution of position error and retinal slip during single trials of visual tracking. The onset of step-ramp motion is denoted in circles and saccade trigger times are denoted in diamonds. During smooth trials (Fig. 8, black trace), position error and retinal slip values lead to subthreshold saccade confidence for the

entirety of the trial. During foveofugal target motion (Fig. 8, red trace), position error and retinal slip values lead to high saccade confidence and rapid saccade trigger. During some cases of foveopetal target motion (Fig. 8, blue traces), the initial step-ramp results in low saccade confidence, which eventually increases to threshold with the subsequent pursuit movement. This explains why long trigger times tend to cluster around the limits of the smooth zone (Fig. 7), since these trials begin with low saccade confidence that ultimately evolves toward threshold confidence much later in the pursuit trajectory.

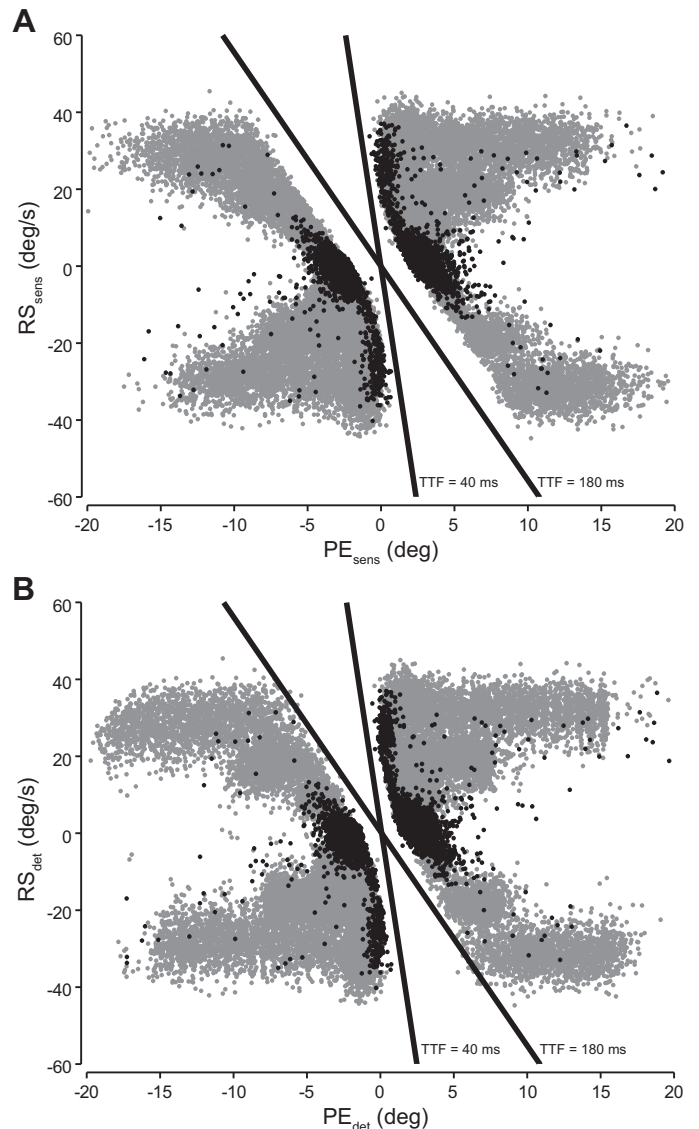


**Figure 7.** Phase plot illustrating retinal slip vs. position error values at time of simulated saccade trigger. *A*: sensory RS vs PE. *B*: true RS vs. PE measured  $70$  ms (visual delay) prior to saccade trigger time. Solid lines represent constant TTF values. Gray dots indicate regular latency saccades, whereas black dots indicate saccades with trigger time greater than  $300$  ms. The model replicates the minimization of saccade trigger when TTF is between  $40$  ms and  $180$  ms and the occurrence of long latency saccades near this smooth zone. det, deterministic (true value); PE, position error; RS, retinal slip; sens, sensory estimate; TTF, time-to-foveation.

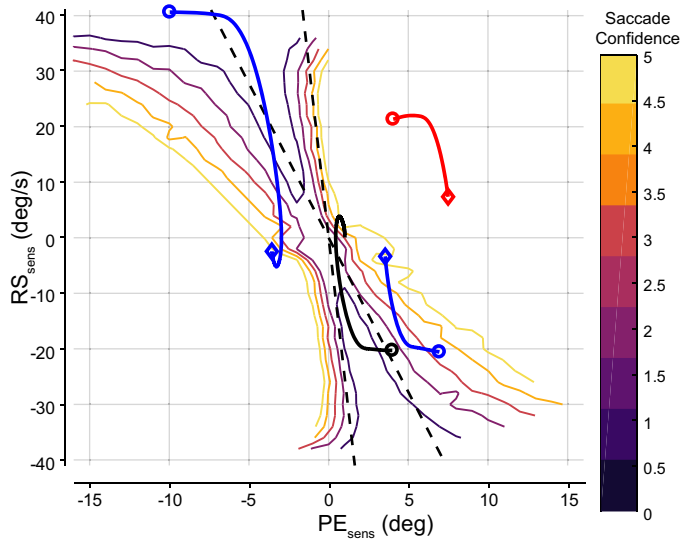


**Figure 8.** Phase plot illustrating average saccade confidence as a function of position error and retinal slip and the evolution of position error and retinal slip in single trials (onset marked by circle, saccade marked by diamond). Time-to-foveation limits of the smooth zone are plotted as straight dashed lines. Pursuing a foveopetal target with a 2-deg step and  $-20$  deg/s ramp (black) does not trigger a saccade as the combined pursuit and target motion result in low saccade confidence values. Pursuing a foveofugal target with a 2-deg step and 20-deg/s ramp (red) leads to an early saccade since the initial saccade confidence is high and is not reduced by subsequent pursuit. Pursuing a foveopetal target with a 7-deg step and  $-20$  deg/s ramp (blue, bottom right quadrant) results in low initial saccade confidence that eventually increases to threshold during subsequent pursuit, resulting in a long trigger time. Similarly, foveopetal target motion with  $-10$  deg step and 40 deg/s ramp (blue, top left quadrant) results in initial smooth tracking followed by late trigger time after exiting the smooth zone. PE, position error; RS, retinal slip.

### New Model Predictions

Our model makes a series of novel predictions. First, the absolute value of velocity change should correlate with saccade frequency and trigger time beyond the relationship described by the time-to-foveation parameter. Figure 9 illustrates saccade proportion (Fig. 9A) and mean saccade trigger time (Fig. 9B) as a function of time-to-foveation (TTF), sorted by velocity step for step-ramp motion during sustained pursuit. For larger changes in velocity, more position error accumulates over time as the eye accelerates to match target speed, resulting in more frequent trials with saccade trigger (Fig. 9A). However, this also results in more uncertainty in predicted position error (contributed by signal-dependent noise in retinal slip), and longer trigger times (Fig. 9B). For smaller velocity changes near the smooth zone, the saccade decision is more strongly driven by initial sensory position error. Thus, although these conditions have less trials with saccade trigger (Fig. 9A), trials with saccade trigger tend to occur earlier (Fig. 9B), particularly if the step-ramp related increase in position error matches the direction of any preexisting steady-state position error.

A second novel prediction from this model is that increasing the uncertainty of position error estimates will impact saccade decision-making during pursuit. Increasing predicted position noise can be achieved experimentally through Gaussian blurring of the pursuit target and

implemented in the model through an increase of the noise corrupting sensory observations. Specifically, we predict a decrease in saccade frequency and an increase in the variability of saccade trigger time in response to step-ramp target trajectories with time-to-foveation near the smooth zone (Fig. 10B) but a minimal impact on saccade trigger time distributions for negative time-to-foveation trajectories (corresponding to a position step and velocity change in the same direction; Fig. 10A). This is because the smooth zone corresponds to retinal motion resulting in low predicted PE and saccade confidence is highly sensitive to sensory uncertainty for small predicted PE values (as demonstrated schematically in Fig. 3). When time-to-foveation values are outside the smooth zone and positive (Fig. 10C), there is a decrease in the proportion of early saccades and an increase in the proportion of late saccade. This is explainable by a widening in the low saccade confidence valley illustrated in the phase plot in Fig. 8, where the early trajectory tends to occur in regions with low saccade confidence while eventually exiting this low-confidence valley, as RS is driven to zero but predicted PE remains nonzero. Overall, increasing sensory uncertainty widens the range of tolerable position error estimates that fail to trigger saccades.

To further motivate the parallels between our model and oculomotor neurophysiology, we simulated a replication of a cortical microstimulation study to predict saccade frequency and trigger time distributions. In this experimental study,

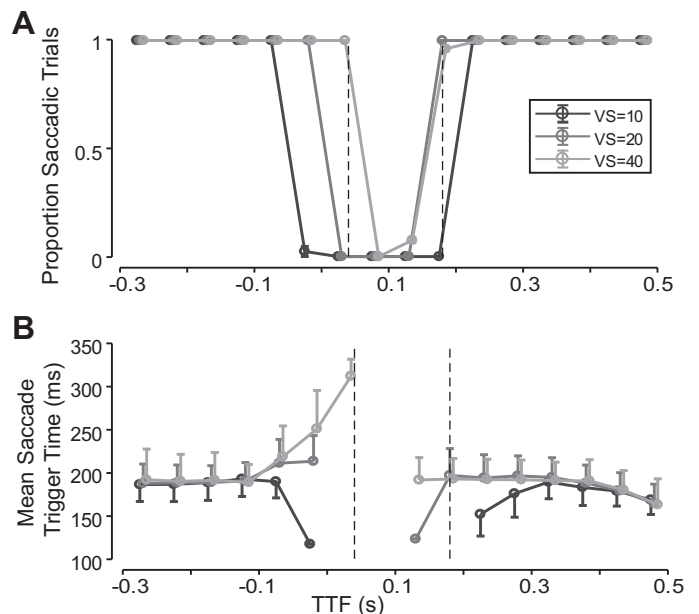


**Figure 9.** Summary statistics of simulated step-ramp target motion during steady-state pursuit following initial Rashbass step-ramp. **A:** proportion of trials with at least one saccade ( $\pm$ SE) plotted against time-to-foveation (TTF) and separated by absolute values of change in target speed. Recall that  $TTF = -PE/RS$ . For identical time-to-foveation conditions, probability of saccade trigger is higher for larger changes in target speed exclusively around the smooth zone (defined as time-to-foveation values between 40 and 180 ms, delimited by the two vertical dashed lines). **B:** mean saccade trigger time ( $\pm$ SD) plotted against TTF, separated by absolute value of change in target speed. For identical time-to-foveation conditions, saccade trigger time increases with increasing change in target speed, especially around the smooth zone. PE, position error; RS, retinal slip; VS, velocity step.

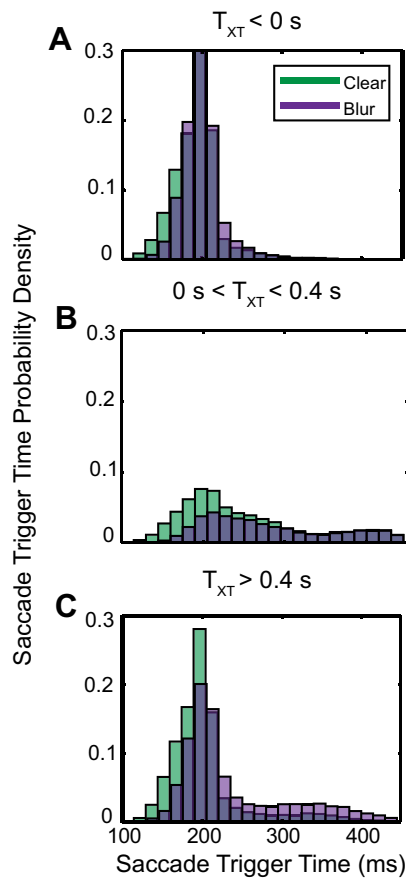


**Figure 10.** Saccade trigger time probability distributions sorted by target-crossing time for typical and unusually high sensory position uncertainty grouped by target-crossing time ( $T_{XT} = -\text{position step}/\text{velocity step}$ ). **A:** increasing sensory noise has minimal influence on saccade trigger time distributions for negative  $T_{XT}$  target motion conditions. **B:** this range of  $T_{XT}$  values are near the smooth zone, where saccade execution is minimized. With increasing sensory noise there is a further reduction in saccade probability and increased variability in saccade trigger time. **C:** with positive  $T_{XT}$  values beyond the smooth zone, there is an increase in saccade trigger time variability with increased sensory noise, including an increased probability of late trigger times between 300 ms and 400 ms.

Groh et al. (83) applied microstimulation to middle temporal area (MT) in macaque monkeys during step-ramp target tracking. They found that microstimulation evoked an effective retinal slip vector that systematically modulated both pursuit velocity and saccade vector and had a complex (but not analyzed) influence on saccade latency that depended on the ongoing target motion. Here, we simulated the effects of microstimulation to area MT by fixing the value of sensory RS (i.e., output from Kalman filtering in Fig. 1) during a static target step. We replicate their observations when the stimulated RS vector is opposite the target position step and make novel predictions for the case that the stimulated RS and target position step are in the same direction. Figure 11 illustrates single trials of tracking a high contrast, static target step in control versus MT microstimulation condition in macaque monkey experimental data (Fig. 11, A and B) and model simulations (Fig. 11, C and D). In model simulations, the stimulated RS is +10 deg/s, matching the electrically evoked RS vectors in Ref. 83. When the stimulated RS vector is opposite to the target step (foveopetal, blue, as in 83), this

drives pursuit in the direction opposite to the step (increasing true PE) but extrapolates the target position toward the fovea (decreasing predicted PE). This results in low predicted position error (Fig. 11D) and long, variable saccade trigger times in the stimulation compared with control condition (Fig. 12A, dark green versus light green/purple). When the stimulated RS is in the same direction as the target step (Fig. 11, B and D, red trace, novel prediction), predicted PE is larger than the true PE, resulting in overshooting saccade amplitudes, but the ceiling effects on the increase in saccade confidence (as illustrated in Fig. 3, C and D) results in similar distributions of trigger times (Fig. 12A, dark purple versus light green/purple).

We additionally investigated how saccade behavior in this simulated microstimulation paradigm changes with increased sensory uncertainty. As shown before, simulating increased sensory position noise (corresponding to a blurred target) increased the mean and variability of trigger time distributions (Fig. 12B). When the target step was in the opposite direction as the stimulated RS vector (dark green), there was a large increase in mean and variability of trigger time distributions. When stimulated RS vector was in the same direction as the step (dark purple), there was a reduction in mean and variability of trigger time distributions. Thus our model predicts how sensory estimates and uncertainties in position error and retinal slip interact in the decision to trigger saccades following cortical microstimulation in motion sensitive area MT, demonstrating that our model is compatible with known neurophysiology of the oculomotor system and can predict behavioral consequences of neurophysiological interventions.

### Effects of Decision Parameter Variations

To illustrate the influence of model parameters within the decision mechanism on saccade behavioural outcomes, we simulated pursuit initiation for a step-ramp target with a velocity of -20 deg/s and position steps between -4 and 10 degrees while varying model parameters (i.e., accumulator time constant, decision threshold, sensory extrapolation time). With this target speed, saccades are expected to be minimized (i.e., smooth zone) when the target step is 4 degrees (12). When increasing the accumulator time constant (Fig. 13, A and B), instantaneous changes in predicted position error (and its estimated variance) have a weaker influence (i.e., integrated with lower weight) on the evolution of saccade confidence (Eq. 12). This results in a pervasive increase in saccade trigger time regardless of target step size (Fig. 13B) and widening of the smooth zone (Fig. 13A), where larger transient predicted position error values can be tolerated without saccade execution. By increasing the decision threshold (Fig. 13, C and D), more accumulated evidence of predicted position error is required before triggering saccades. This leads to a slight widening of the smooth zone (Fig. 13C) and slight increase in saccade trigger time around the smooth zone (Fig. 13D). Finally, increasing the motion extrapolation time to compute predicted position error (Fig. 13, E and F) results in a shift and widening of the smooth zone (Fig. 13E). Furthermore, the range of position steps near the smooth zone producing saccades with long trigger time is widened (Fig. 13F), which is caused by the increased

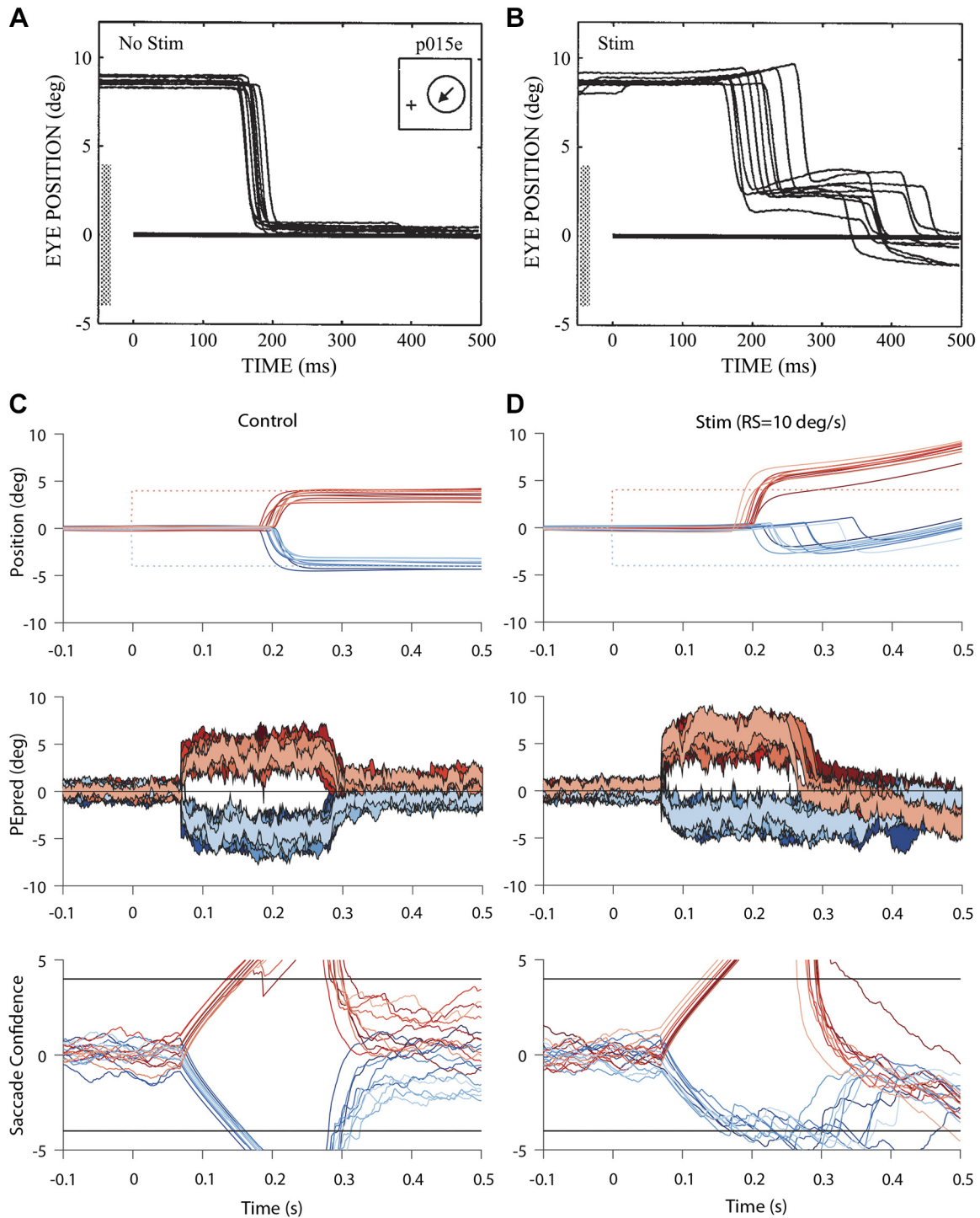


**Figure 11.** A and B: experimental data from macaques performing saccades to static steps in control (A) and MT microstimulation (B) conditions (Figure from Ref. 83, Copyright 1997 Society for Neuroscience). C and D: single trial simulations using a static target step (+4 deg in red, -4 deg in blue) in control (C) and microstimulation (D) conditions. In the control condition, estimated RS has a mean value around zero (the true value). Predicted PE (PEpred) and saccade confidence are driven by the target position step, resulting in rapid, low-variability saccade trigger times. In Stim condition, the estimated RS was fixed to +10 deg/s, corresponding to stimulation of MT as performed by Groh et al. (83). When the stimulated RS vector was opposite to the target step (blue, as in 83), PEpred is extrapolated towards zero. This results in a reduction of saccade confidence over time, producing saccade with longer and more variable trigger time with undershooting saccade amplitude. When the stimulated RS vector was in the same direction as the target step (red, novel prediction) predicted PE is larger, but this results in similar evolution of saccade confidence and similarly rapid and regular saccade trigger times with overshooting saccade amplitude. MT, middle temporal area; PE, position error; RS, retinal slip.

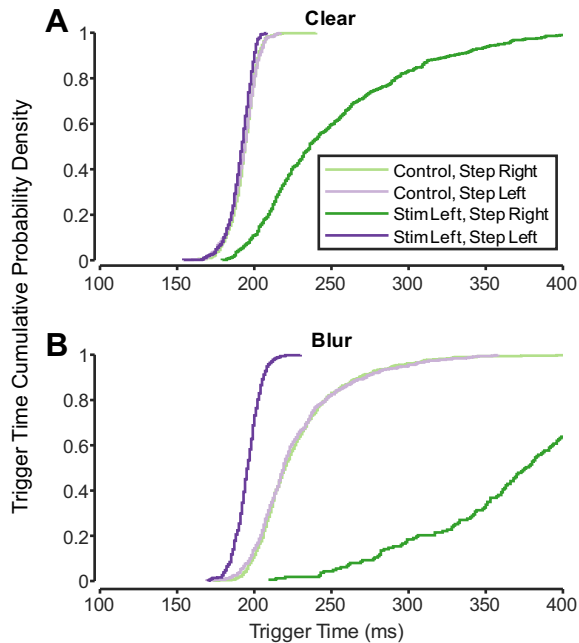


**Figure 12.** Trigger time distributions for clear and blur target conditions using  $\pm 4$ -deg target step and 10-deg/s stimulated RS vector. **A:** with a clear target, a stimulated RS vector opposite to the step (dark green) caused an increase in the mean and variability of the trigger time distribution compared with control (light purple, light green), while a stimulated RS vector in the same direction as the step (dark purple) had little effect on trigger time distribution compared with control. **B:** with a blurred target, the trigger time distribution in control condition had a larger mean and variance compared with the clear target control. When the stimulated RS vector was in the same direction as the target step (dark purple), there was a reduction in mean and variability of the trigger time distribution compared with control, while a stimulated RS vector opposite to the target step (dark green) further increased the mean and variability of the trigger time distribution compared with control. RS, retinal slip; stim, simulated middle temporal area microstimulation.

uncertainty contributed by the motion pathway (Eq. 9). The same trends hold for saccades during sustained pursuit (not shown).

Using experimental data from human visually tracking step-ramp targets (61), we used maximum likelihood estimation to estimate optimal fits for decision-making parameters to test the validity of our choices of parameter values used in this modeling study. These fitted values are reported in Table 2. This confirms that our default model parameter values fell within the range of participants individual model fit values; however, individual participants parameters were quite variable.

## DISCUSSION

In this model of saccadic decision-making during pursuit, confidence in predicted position error triggers saccades upon accumulating to a threshold value. Position error is predictively estimated from noisy and delayed sensory observations to compute the evidence that the target is outside the fovea (saccade confidence, quantified through log-probability ratio). This decision mechanism reproduces the Rashbass paradigm (12), as well as the empirical relationships between time-to-foveation and saccade execution and trigger time (Figs. 4–8) (13, 14). The model makes novel

predictions about the relationship between target trajectory and saccade behavior that cannot be accounted by time-to-foveation correlations. Specifically, families of step-ramp target motion with identical time-to-foveation should evoke saccades with longer trigger times near the smooth zone (time-to-foveation between 40 and 180 ms) (14) as changes in target speed increases (Fig. 9). The model makes further predictions that increasing sensory uncertainty, such as by blurring the visual target (33), will further reduce the probability of saccade trigger and increase saccade trigger time variability during pursuit, particularly during conditions of low predicted position error (near the smooth zone; Fig. 10). Furthermore, the model makes novel predictions about saccade amplitudes and trigger time distributions in a simulated replication of an area MT cortical microstimulation study (83) (Figs. 11 and 12). Finally, we demonstrate through empirical model fitting that our choices in model parameters fit the range of human participants (Table 2) and demonstrate the behavioral effects of variation in model parameters (Fig. 13).

## Model Limitations

This model focuses on the visual basis of saccadic decision-making during pursuit without considering the influence of learning and selective attention. In testing saccade behavior at pursuit initiation, Bieg et al. (13) randomized the timing, position step size, and motion direction but not motion speed of the target. This could allow for learning speed priors that modify the initial trajectory (and therefore ongoing sensory signals) during the initial pursuit acceleration (84–86). In contrast, de Brouwer et al. (14) randomized all aspects of target motion at the second step-ramp, attempting to minimize the influence of learning and expectation, thus providing a more ideal data set for evaluating modeled trigger time distributions. However, selective attention may also present a confounding influence even in the absence of learned expectations. It has been shown that attention is preferentially allocated ahead of pursuit (87, 88), which can preferentially enhance the precision of sensory signals (89). Furthermore, attention may have more direct effects on oculomotor behavior (90, 91), possibly through influencing normative decision thresholds (92) or accumulation rates (93). Nevertheless, previous modeling studies have demonstrated a dominant influence of sensory variability driving pursuit variability (5), suggesting this model captures the dominant influences on saccade behavior despite omitting potential cognitive influences. Although the mechanisms by which these cognitive factors impact saccadic decision-making warrants further investigation, the model successfully illustrates principles of saccade-pursuit coordination and its sensory influences.

Another current limitation that could be addressed in future research is how evolving sensory signals may influence saccade programming after saccade trigger. Although it has been clearly shown that saccade amplitude accounts for both position error and retinal slip (54, 56, 60), the influence of retinal slip on saccade amplitude and direction can asynchronously influence the later component of the saccade as demonstrated by curved saccades during two dimensional tracking (82). Similarly, when saccade targets are abruptly

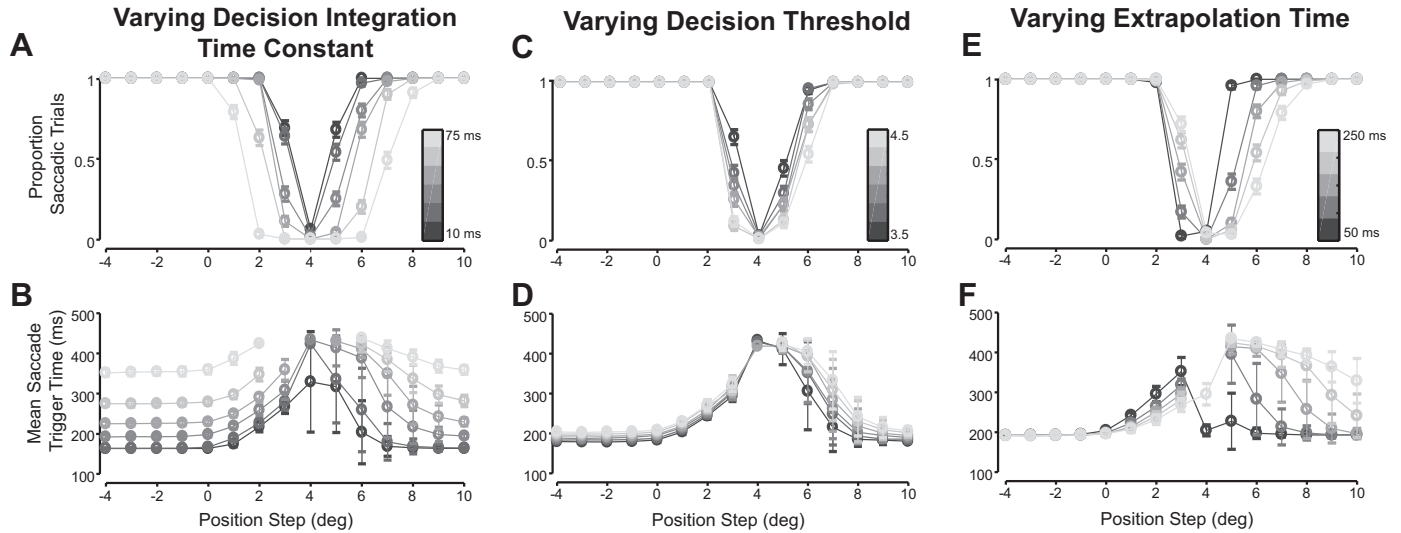


**Figure 13.** Effects of decision parameter variation on saccade proportion and saccade trigger time during pursuit initiation with a target velocity of  $-20$  deg/s and varying position steps. For these simulations, all other parameters were held at constant, default values. Based on (12), saccade frequency should be minimized with a position step of 4 deg. **A:** increasing the value of the leaky integration time constant in the saccade confidence accumulator (darkest gray corresponds to time constant of 5 ms; lightest gray corresponds to time constant of 50 ms) leads to a widening smooth zone. **B:** increasing the value of the leaky integration time constant leads to increased saccade trigger time for all position steps, including far beyond the smooth zone. **C:** increasing the value of the saccade confidence decision threshold (darkest gray corresponds to threshold of 3.5, lightest gray corresponds to a threshold of 4.5) results in decreasing saccade proportion near the smooth zone, and a slight widening of smooth zone. **D:** increasing the value of the decision threshold leads to slight increases in saccade trigger time only near the smooth zone. **E:** increasing sensory extrapolation time shifts the smooth zone (darkest gray corresponds to extrapolation time of 50 ms, lightest gray corresponds to extrapolation time of 250 ms). **F:** increasing sensory extrapolation time increases saccade trigger time near the smooth zone.

displaced before saccade onset, saccade trajectories may initially aim toward the initial target position then curve mid-flight toward the final target location (94, 95). This suggests saccade programming is not limited to the information at saccade trigger time, but can still incorporate visual information that only becomes available subsequently (due to delays). Furthermore, during countermanding tasks, erroneously executed saccades have a latency-dependent reduction in amplitude (96), suggesting that the stop signal can still influence amplitude programming even after saccade trigger time. These modifications and curvatures in saccade trajectory have been linked to evolving position error estimates after saccade trigger time (97–99). Thus, a potentially interesting extension of this model could investigate how changes in post-trigger predicted position error could influence saccade trajectories.

### Bounded Evidence Accumulation and Confidence Estimation in Decision-Making

We have applied the framework of recurrent Bayesian estimation and bounded evidence accumulation toward modeling saccadic decision-making in an oculomotor control task. This modeling framework has previously been successfully

applied to perceptual decision-making, simulating choices, reaction times, and postdecision confidence (25). Recently, the concept of confidence estimation has been considered central to the decision process itself (100–102), reflecting the posterior probability that an action is appropriate given the accumulated evidence and potential biases/priors (36). Confidence has been shown to evolve dynamically over the course of evidence accumulation (103) and acts as a critical quantity in multisensory (104) and multistage (105) decision-making. The agreement between model simulations and data suggests the important role of confidence estimation in saccade trigger during pursuit. Thus, we validate previous perceptual decision theory in a novel oculomotor control domain, demonstrating that confidence estimation is also a fundamental principle in motor coordination.

### Generalizability of Saccade Confidence as a Decision Variable

A major feature of the proposed decision mechanism is the generalizability of saccade confidence as a decision variable compared with the previously hypothesized time-to-foveation parameter. Recall that time-to-foveation is defined as the negative ratio between position error and retinal slip.

**Table 2.** Value of decision parameters used in model simulations and estimated parameter fits from empirical data (61)

Parameter Name	Parameter Symbol	Parameter Value in Main Simulations	Empirical Fitted Value (Means $\pm$ SD)	Range of Empirical Fitted Values
Motion extrapolation time constant	$T_{sacc}$	125 ms	$71 \pm 34$ ms	8–142 ms
Decision integration time constant	$\tau_s$	25 ms	$13 \pm 5.6$ ms	6.6–27 ms
Decision threshold	$\theta_{saccade}$	4	$6.5 \pm 1.2$	3.9–7.9

This value rapidly grows to infinity as retinal slip approaches zero. Thus, although the parameter correlates with saccade behavior after an abrupt change in target motion (14), it is unsuitable as a decision variable for general saccade trigger. In contrast, the mechanism proposed here can explain saccade trigger to both stationary and moving targets.

The proposed decision mechanism comparing the evidence of the target being on opposite sides of the fovea was inspired by the topographic organization of excitatory and inhibitory lateral connections across the superior colliculus (106) and physiological evidence that fixational stability results from balanced neural activity in populations with opposing movement tendencies (107). An alternative model comparing the evidence of the target being inside versus outside the fovea requires defining an explicit foveal deadzone for saccade trigger (108). Instead, our mechanism lacks an explicit deadzone, so the size of the smallest possible saccades is only limited by the uncertainty in predicted position error, agreeing with evidence toward a common neural mechanism underlying the control of saccades and microsaccades (109, 110).

The model is also compatible with extensions to describe saccade trigger during visual tracking of two-dimensional target motion. This is in contrast with the time-to-foveation model, which is based on the linear extrapolation and intersection of eye and target trajectories in time; however, eye and target trajectories do not generally intersect in two-dimensional motion. In our framework, a similar saccade confidence estimator may compute the log-probability ratio of the target being above versus below the fovea. These confidence estimators could then be combined to additionally account for vertical and oblique saccade trigger. A challenge would be that independently estimating horizontal and vertical components results in a loss of estimated covariance information. One solution that optimally accounts for covariance is estimating two-dimensional saccade confidence through the Mahalanobis distance (111, 112) between the fovea and the probabilistic estimate of predicted position error. This measure provides a normalized distance similar to a  $z$ -score, uniquely specifying the probability that a reference point (e.g., the fovea) falls within a multivariate distribution (e.g., 2D predicted position error). Using probabilistic population coding, this log-probability ratio could be implemented through a linear read-out from the two-dimensional representation of predicted position error (see next section for details). Thus, the Mahalanobis distance could provide an efficient computational (normative) mechanism enabling a sequential probability ratio test to estimate saccade confidence in two-dimensional tracking.

### Neurophysiological Implementation

Our model normatively outlines the computational steps underlying saccadic decisions, which has implications on the signals and connectivity of its neural implementation. We thus find it useful to speculate on its potential neurophysiological implementation. First, the model suggests that motion and position information must converge into a predictive position error estimate that ultimately informs the saccade decision process. Motion information supplied by the middle temporal area (MT) has been shown to causally

influence saccade metrics and latency (83, 113). Activity in the superior colliculi (SC) indicates position error during pursuit (114, 115) and causally influences saccade trigger during pursuit (116, 117). MT and SC both communicate with the frontal eye fields (118, 119), an area involved in predictive oculomotor control (120, 121). Neurons in this area contain the necessary position and motion information to support this predictive saccade decision (52, 122). Similarly, the lateral intraparietal area (LIP) is interconnected with MT and FEF and has also been implicated in oculomotor control and evidence accumulation (123–126). Neuronal activity in FEF and LIP predicts saccade choice and timing consistent with bounded accumulator models (127, 128). Models suggest that neural pathway from FEF through the caudate nucleus terminating in the SC is capable of reading out threshold crossing to trigger saccades (91, 129).

Brain regions in this distributed, interconnected oculomotor network might represent information through probabilistic population activity (130). This representation allows encoding of uncertainty information that can be used to drive efficient probabilistic computations. For example, if this population variability is Poisson-like, then log-likelihood ratios can be computed from linearly-weighted population readouts (131, 132). An alternative hypothesis suggests that the dynamics of neuronal population responses sample the inferred posterior distribution, where estimated uncertainty is encoded through temporal variability of neural population activity (133). Both neural implementations allow time-varying estimates of uncertainty and thus both are compatible with our proposed saccade decision model, although they have different implications about how this information should be read-out (linear versus nonlinear decoding) by downstream neural circuits. Although the hypothesis that the position error information represented in the SC can be predictively motion extrapolated remains unsettled (114, 134, 135), a unified Poisson-like probabilistic population representation of PE<sub>pred</sub> would allow the probability favoring a saccade (Eq. 10) to be computed by a linear readout. The comparison between  $P_k^{Left}$  and  $P_k^{Right}$  in Eq. 11 could be performed through the reciprocal inhibition between left and right SC (and medial versus lateral SC when considering two-dimensional tracking) (106, 107). Single-neuron recordings in the rostral SC (corresponding to foveal target positions) suggest shifting PE tuning curves with target motion (114, see their Fig. 11, C and D). Thus, relating PE<sub>pred</sub> in our model with the distribution of activity in the SC seems to unify the observations that both increased spatial blurring of a single target (136) or using larger targets arrays (137) diminish the frequency of catch-up saccades by increasing PE<sub>pred</sub> uncertainty in our model or increasing the spread of neural activity between the left and right rostral SC. Thus, the proposed decision mechanism comparing the probabilities  $P^{Left}$  and  $P^{Right}$  implements the “dynamic equilibrium” hypothesis (107), rather than a dedicated “fixation zone” in the rostral SC (138).

### Prediction and Confidence Estimation in General Motor Coordination

Prediction in coordinated motor decisions is pervasive in our daily lives. For example, when manually intercepting a

moving object, humans predictively direct their reaching movements to account for sensorimotor delays and object motion (139–142). Prior to executing the reach, saccades are typically directed to this predicted target location (143, 144), and both movements have correlated timing and end point error (145). This suggests that both eye and arm movement metrics are programmed by a common internal representation of the predicted target trajectory (146), and we suggest that similar confidence-based decision strategies may explain the trigger time for interceptive reaching decisions. Thus, prediction is an important component in ensuring accurate movements, and confidence estimation can evaluate the appropriateness of a particular action given the uncertainty of the predicted state.

Similar coordinated movements occur in a variety of animal species, who may also utilize similar decision principles in coordinating movements from delayed and uncertain sensory signals. For example, flies (*Drosophila*) in visually guided flight perform coordinated smooth and saccadic turning to accurately orient toward their flight goal (147). Models including temporal integration of motion information have been used to explain this rapid decision-making (148), but it has not yet been investigated how uncertainty in visual motion may influence these decisions. As another example, zebrafishes integrate specific visual features in the perceptual decision of prey recognition, which can initiate hunting routines such as convergent saccades, orienting turns, and capture swims (149). The visual features important to prey detection have been described (150), and the neural circuits mediating prey recognition and the initiation of hunting have been localized to nonoverlapping populations in the optic tectum (151–153). Spontaneous tectal activity independent from retinal inputs, rather than being random noise fluctuations, has been shown to match the patterns of activity evoked by ethologically relevant visual stimuli (154). This structured spontaneous activity can be interpreted as Bayesian priors to enabling efficient stochastic decision-making for coordinated orienting responses (155), although more research is needed into how this structured, stochastic population activity can robustly coordinate orienting responses. Thus, principles from our model can be combined with the advanced experimental techniques in these model animals (156–158) for detailed investigation on the neural implementation of predictive decision-making and motor coordination.

## CONCLUSIONS

Our model of saccade decision-making during pursuit handles the constraints of delay and signal-dependent noise in the oculomotor system while reproducing established trends in saccade frequency and trigger time across a range of target motion trajectories. The model illustrates how discretely triggered orienting movements like saccades can be coordinated during continuously controlled pursuit through predictive, probabilistic evidence (confidence) accumulation. We suggest that this framework of prediction and confidence estimation represents a fundamental principle in stochastic decision-making for sensorimotor coordination.

## GRANTS

This work was supported by the National Sciences and Engineering Research Council (Canada) and the Canada Foundation for Innovation.

## DISCLOSURES

No conflicts of interest, financial or otherwise, are declared by the authors.

## AUTHOR CONTRIBUTIONS

J.D.C., P.L., and G.B. conceived and designed research; J.D.C. performed experiments; J.D.C. analyzed data; J.D.C., P.L., and G.B. interpreted results of experiments; J.D.C. prepared figures; J.D.C. drafted manuscript; J.D.C., P.L., and G.B. edited and revised manuscript; J.D.C., P.L., and G.B. approved final version of manuscript.

## REFERENCES

1. Keller EL, Heinen SJ. Generation of smooth-pursuit eye movements: neuronal mechanisms and pathways. *Neurosci Res* 11: 79–107, 1991. doi:10.1016/0168-0102(91)90048-4.
2. Lisberger SG. Visual guidance of smooth pursuit eye movements. *Annu Rev Vis Sci* 1: 447–468, 2015. doi:10.1146/annurev-vision-082114-035349.
3. Faisal AA, Selen LPJ, Wolpert DM. Noise in the nervous system. *Nat Rev Neurosci* 9: 292–303, 2008. doi:10.1038/nrn2258.
4. van Beers RJ, Baraduc P, Wolpert DM. Role of uncertainty in sensorimotor control. *Philos Trans R Soc Lond B Biol Sci* 357: 1137–1145, 2002. doi:10.1098/rstb.2002.1101.
5. Osborne LC, Lisberger SG, Bialek W. A sensory source for motor variation. *Nature* 437: 412–416, 2005. doi:10.1038/nature03961.
6. Diaz GJ, Cooper J, Hayhoe MM. Memory and prediction in natural gaze control. *Philos Trans R Soc Lond B Biol Sci* 368: 20130064, 2013. doi:10.1098/rstb.2013.0064.
7. Ke SR, Lam J, Pai DK, Spering M. Directional asymmetries in human smooth pursuit eye movements. *Invest Ophthalmol Vis Sci* 54: 4409–4421, 2013. doi:10.1167/iovs.12-11369.
8. Krauzlis RJ. Recasting the smooth pursuit eye movement system. *J Neurophysiol* 91: 591–603, 2004. doi:10.1152/jn.00801.2003.
9. Orban de Xivry J-J, Lefèvre P. Saccades and pursuit: two outcomes of a single sensorimotor process. *J Physiol* 584: 11–23, 2007. doi:10.1113/jphysiol.2007.139881.
10. Huys R, Studenka BE, Rheaume NL, Zelaznik HN, Jirsa VK. Distinct timing mechanisms produce discrete and continuous movements. *PLoS Comput Biol* 4: e1000061, 2008. doi:10.1371/journal.pcbi.1000061.
11. Huys R, Jirsa VK, Studenka BE, Rheaume N, Zelaznik HN. Human trajectory formation: taxonomy of movement based on phase flow topology. In: *Coordination: Neural, Behavioral and Social Dynamics*, edited by Fuchs A, Jirsa VK. Berlin, Heidelberg: Springer, 2008, p. 77–92. doi:10.1007/978-3-540-74479-5\_4.
12. Rashbass C. The relationship between saccadic and smooth tracking eye movements. *J Physiol* 159: 326–338, 1961. doi:10.1113/jphysiol.1961.sp006811.
13. Bieg HJ, Chuang LL, Bühlhoff HH, Bresciani JP. Asymmetric saccade reaction times to smooth pursuit. *Exp Brain Res* 233: 2527–2538, 2015. doi:10.1007/s00221-015-4323-8.
14. de Brouwer S, Yuksel D, Blohm G, Missal M, Lefèvre P. What triggers catch-up saccades during visual tracking? *J Neurophysiol* 87: 1646–1650, 2002. doi:10.1152/jn.00432.2001.
15. Chang C-J, Zajayeri M. Integration of speed and time for estimating time to contact. *Proc Natl Acad Sci USA* 115: 201713316, 2018. doi:10.1073/pnas.1713316115.
16. Lee DN. A theory of visual control of braking based on information about time-to-collision. *Perception* 5: 437–459, 1976. doi:10.1068/p050437.

17. **Regan D, Gray R.** Visually guided collision avoidance and collision achievement. *Trends Cogn Sci* 4: 99–107, 2000. doi:10.1016/S1364-6613(99)01442-4.
18. **Carpenter RH, Williams MLL.** Neural computation of log-likelihood in control of saccadic eye movements. *Nature* 377: 59–62, 1995. doi:10.1038/377059a0.
19. **Gold JI, Shadlen MN.** Neural computations that underlie decisions about sensory stimuli. *Trends Cogn Sci* 5: 10–16, 2001. doi:10.1016/S1364-6613(00)01567-9.
20. **Hanks TD, Summerfield C.** Perceptual decision making in rodents, monkeys, and humans. *Neuron* 93: 15–31, 2017. doi:10.1016/j.neuron.2016.12.003.
21. **Ratcliff R.** A theory of memory retrieval. *Psychol Rev* 85: 59–108, 1978. doi:10.1037/0033-295X.85.2.59.
22. **Vickers D.** *Decision Processes in Visual Perception.* New York: Academic Press Inc, 1979.
23. **Fetsch CR, Odean NN, Jeurissen D, El-Shamayleh Y, Horwitz GD, Shadlen MN.** Focal optogenetic suppression in macaque area MT biases direction discrimination and decision confidence, but only transiently. *eLife* 7: e36532, 2018. doi:10.7554/eLife.36523.
24. **Fetsch CR, Kiani R, Newsome WT, Shadlen MN.** Effects of cortical microstimulation on confidence in a perceptual decision. *Neuron* 83: 797–804, 2014 [Erratum in *Neuron* 84: 239, 2014]. doi:10.1016/j.neuron.2014.07.011.
25. **Fetsch CR, Kiani R, Shadlen MN.** Predicting the accuracy of a decision: a neural mechanism of confidence. *Cold Spring Harb Symp Quant Biol* 79: 185–197, 2014. doi:10.1101/sqb.2014.79.024893.
26. **Gold JI, Shadlen MN.** The neural basis of decision making. *Annu Rev Neurosci* 30: 535–574, 2007. doi:10.1146/annurev.neuro.29.051605.113038.
27. **Schall JD.** Macrocircuits: decision networks. *Curr Opin Neurobiol* 23: 269–274, 2013. doi:10.1016/j.conb.2012.11.009.
28. **Schall JD.** Decision making: from sensory evidence to a motor command. *Curr Biol* 10: R404–R406, 2000. doi:10.1016/S0960-9822(00)00504-2.
29. **van den Berg R, Anandalingam K, Zylberberg A, Kiani R, Shadlen MN, Wolpert DM.** A common mechanism underlies changes of mind about decisions and confidence. *eLife* 5: e12192, 2016. doi:10.7554/eLife.12192.
30. **Krauzlis RJ, Lisberger SG.** A model of visually-guided smooth pursuit eye movements based on behavioral observations. *J Comput Neurosci* 1: 265–283, 1994. doi:10.1007/BF00961876.
31. **Bogadhi AR, Montagnini A, Masson GS.** Dynamic Interaction between retinal and extra-retinal signals in motion integration for smooth pursuit. *J Vis* 13: 5, 2013. doi:10.1167/13.13.5.
32. **Orban de Xivry J-J, Coppe S, Blohm G, Lefèvre P.** Kalman filtering naturally accounts for visually guided and predictive smooth pursuit dynamics. *J Neurosci* 33: 17301–17313, 2013. doi:10.1523/JNEUROSCI.2321-13.2013.
33. **Deravet N, Blohm G, Orban de Xivry J-J, Lefèvre P.** Weighted integration of short-term memory and sensory signals in the oculomotor system. *J Vis* 18: 16, 2018. doi:10.1167/18.5.16.
34. **Forstmann BU, Ratcliff R, Wagenmakers E-J.** Sequential sampling models in cognitive neuroscience: advantages, applications, and extensions. *Annu Rev Psychol* 67: 641–666, 2016. doi:10.1146/annurev-psych-122414-033645.
35. **Wald A, Wolfowitz J.** Optimum character of the sequential probability ratio test. *Ann Math Statist* 19: 326–339, 1948. doi:10.1214/aoms/1177730197.
36. **Pouget A, Drugowitsch J, Kepecs A.** Confidence and certainty: distinct probabilistic quantities for different goals. *Nat Neurosci* 19: 366–374, 2016. doi:10.1038/nn.4240.
37. **Beck JM, Ma WJ, Kiani R, Hanks TD, Churchland AK, Roitman JD, Shadlen MN, Latham PE, Pouget A.** Probabilistic population codes for Bayesian decision making. *Neuron* 60: 1142–1152, 2008. doi:10.1016/j.neuron.2008.09.021.
38. **Denève S, Duhamel J-R, Pouget A.** Optimal sensorimotor integration in recurrent cortical networks: a neural implementation of Kalman filters. *J Neurosci* 27: 5744–5756, 2007. doi:10.1523/JNEUROSCI.3985-06.2007.
39. **Ma WJ, Beck JM, Pouget A.** Spiking networks for Bayesian inference and choice. *Curr Opin Neurobiol* 18: 217–222, 2008. doi:10.1016/j.conb.2008.07.004.
40. **Pouget A, Dayan P, Zemel RS.** Inference and computation with population codes. *Annu Rev Neurosci* 26: 381–410, 2003. doi:10.1146/annurev.neuro.26.041002.131112.
41. **Tavassoli A, Ringach DL.** Dynamics of smooth pursuit maintenance. *J Neurophysiol* 102: 110–118, 2009. doi:10.1152/jn.91320.2008.
42. **Harris CM, Wolpert DM.** The main sequence of saccades optimizes speed-accuracy trade-off. *Biol Cybern* 95: 21–29, 2006. doi:10.1007/s00422-006-0064-x.
43. **Harris CM, Wolpert DM.** Signal-dependent noise determines motor planning. *Nature* 394: 780–784, 1998. doi:10.1038/29528.
44. **Nover H, Anderson CH, DeAngelis GC.** A logarithmic, scale-invariant representation of speed in Macaque middle temporal area accounts for speed discrimination performance. *J Neurosci* 25: 10049–10060, 2005. doi:10.1523/JNEUROSCI.1661-05.2005.
45. **Osborne LC, Hohl SS, Bialek W, Lisberger SG.** Time course of precision in smooth-pursuit eye movements of monkeys. *J Neurosci* 27: 2987–2998, 2007. doi:10.1523/JNEUROSCI.5072-06.2007.
46. **Osborne LC, Lisberger SG.** Spatial and temporal integration of visual motion signals for smooth pursuit eye movements in monkeys. *J Neurophysiol* 102: 2013–2025, 2009. doi:10.1152/jn.00611.2009.
47. **van Beers RJ.** The sources of variability in saccadic eye movements. *J Neurosci* 27: 8757–8770, 2007. doi:10.1523/JNEUROSCI.2311-07.2007.
48. **Kalman RE, Bucy RS.** New results in linear filtering and prediction theory. *J Basic Eng* 83: 95–108, 1961. doi:10.1115/1.3658902.
49. **Beck JM, Ma WJ, Pitkow X, Latham PE, Pouget A.** Not noisy, just wrong: The role of suboptimal inference in behavioral variability. *Neuron* 74: 30–39, 2012. doi:10.1016/j.neuron.2012.03.016.
50. **Izawa J, Rane T, Donchin O, Shadmehr R.** Motor adaptation as a process of reoptimization. *J Neurosci* 28: 2883–2891, 2008. doi:10.1523/JNEUROSCI.5359-07.2008.
51. **Todorov E.** Stochastic optimal control and estimation methods adapted to the noise characteristics of the sensorimotor system. *Neural Comput* 17: 1084–1108, 2005. doi:10.1162/0899766053491887.
52. **Cassanello CR, Nihalani AT, Ferrera VP.** Neuronal responses to moving targets in monkey frontal eye fields. *J Neurophysiol* 100: 1544–1556, 2008. doi:10.1152/jn.01401.2007.
53. **de Brouwer S, Missal M, Lefèvre P.** Role of retinal slip in the prediction of target motion during smooth and saccadic pursuit. *J Neurophysiol* 86: 550–558, 2001. doi:10.1152/jn.2001.86.2.550.
54. **Eggert T, Guan Y, Bayer O, Büttner U.** Saccades to moving targets. *Ann N Y Acad Sci* 1039: 149–159, 2005. doi:10.1196/annals.1325.014.
55. **Etchells PJ, Benton CP, Ludwig CJH, Gilchrist ID.** The target velocity integration function for saccades. *J Vis* 10: 7, 2010. doi:10.1167/10.6.7.
56. **Guan Y, Eggert T, Bayer O, Büttner U.** Saccades to stationary and moving targets differ in the monkey. *Exp Brain Res* 161: 220–232, 2005. doi:10.1007/s00221-004-2070-3.
57. **Bennett SJ, Orban de Xivry J-J, Barnes GR, Lefèvre P.** Target acceleration can be extracted and represented within the predictive drive to ocular pursuit. *J Neurophysiol* 98: 1405–1414, 2007. doi:10.1152/jn.00132.2007.
58. **Krauzlis RJ, Lisberger SG.** Temporal properties of visual motion signals for the initiation of smooth pursuit eye movements in monkeys. *J Neurophysiol* 72: 150–162, 1994. doi:10.1152/jn.1994.72.1.150.
59. **Lisberger SG, Westbrook LE.** Properties of visual inputs that initiate horizontal smooth pursuit eye movements in monkeys. *J Neurosci* 5: 1662–1673, 1985. doi:10.1523/JNEUROSCI.05-06-01662.1985.
60. **de Brouwer S, Missal M, Barnes GR, Lefèvre P.** Quantitative analysis of catch-up saccades during sustained pursuit. *J Neurophysiol* 87: 1772–1780, 2002. doi:10.1152/jn.00621.2001.
61. **Nachmani O, Coutinho J, Khan AZ, Lefèvre P, Blohm G.** Predicted position error triggers catch-up saccades during sustained smooth pursuit. *eNeuro* 7: ENEURO.0196-18.2019, 2020. doi:10.1523/ENEURO.0196-18.2019.
62. **Blohm G, Optican LM, Lefèvre P.** A model that integrates eye velocity commands to keep track of smooth eye displacements. *J Comput Neurosci* 21: 51–70, 2006. doi:10.1007/s10827-006-7199-6.
63. **Krauzlis RJ, Miles FA.** Transitions between pursuit eye movements and fixation in the monkey: dependence on context. *J Neurophysiol* 76: 1622–1638, 1996. doi:10.1152/jn.1996.76.3.1622.
64. **Keating EG, Pierre A.** Architecture of a gain controller in the pursuit system. *Behav Brain Res* 81: 173–181, 1996. doi:10.1016/S0166-4328(96)89078-4.

65. **Tabata H, Miura K, Kawano K.** Trial-by-trial updating of the gain in preparation for smooth pursuit eye movement based on past experience in humans. *J Neurophysiol* 99: 747–758, 2008. doi:10.1152/jn.00714.2007.
66. **Mukherjee T, Battifarano M, Simoncini C, Osborne LC.** Shared sensory estimates for human motion perception and pursuit eye movements. *J Neurosci* 35: 8515–8530, 2015. doi:10.1523/JNEUROSCI.4320-14.2015.
67. **Rasche C, Gegenfurtner KR.** Precision of speed discrimination and smooth pursuit eye movements. *Vision Res* 49: 514–523, 2009. doi:10.1016/j.visres.2008.12.003.
68. **Daye PM, Blohm G, Lefèvre P.** Catch-up saccades in head-unrestrained conditions reveal that saccade amplitude is corrected using an internal model of target movement. *J Vis* 14: 12, 2014. doi:10.1167/14.1.12.
69. **Daye PM, Blohm G, Lefèvre P.** Saccadic compensation for smooth eye and head movements during head-unrestrained two-dimensional tracking. *J Neurophysiol* 103: 543–556, 2010. doi:10.1152/jn.00656.2009.
70. **Jürgens R, Becker W, Kornhuber HH.** Natural and drug-induced variations of velocity and duration of human saccadic eye movements: evidence for a control of the neural pulse generator by local feedback. *Biol Cybern* 39: 87–96, 1981. doi:10.1007/BF00336734.
71. **Scudder CA.** A new local feedback model of the saccadic burst generator. *J Neurophysiol* 59: 1455–1475, 1988. doi:10.1152/jn.1988.59.5.1455.
72. **Van Gisbergen JAM, Robinson DA, Gielen S.** A Quantitative analysis of generation of saccadic eye movements by burst neurons. *J Neurophysiol* 45: 417–442, 1981. doi:10.1152/jn.1981.45.3.417.
73. **Bahill AT, Clark MR, Stark LW.** The main sequence, a tool for studying human eye movements. *Math Biosci* 24: 191–204, 1975. doi:10.1016/0025-5564(75)90075-9.
74. **Crevecoeur F, Körding KP.** Saccadic suppression as a perceptual consequence of efficient sensorimotor estimation. *eLife* 6: e25073, 2017. doi:10.7554/eLife.25073.
75. **Goettker A, Braun DI, Schütz AC, Gegenfurtner KR.** Execution of saccadic eye movements affects speed perception. *Proc Natl Acad Sci USA* 115: 2240–2245, 2018. doi:10.1073/pnas.1704799115.
76. **Lisberger SG.** Postsaccadic enhancement of initiation of smooth pursuit eye movements in monkeys. *J Neurophysiol* 79: 1918–1930, 1998. doi:10.1152/jn.1998.79.4.1918.
77. **Robinson DA.** Models of the saccadic eye movement control system. *Biol Cybern* 14: 71–83, 1973. doi:10.1007/BF00288906.
78. **Hu X, Jiang H, Gu C, Li C, Sparks DL.** Reliability of oculomotor command signals carried by individual neurons. *Proc Natl Acad Sci USA* 104: 8137–8142, 2007. doi:10.1073/pnas.0702799104.
79. **Osborne LC.** Computation and physiology of sensory-motor processing in eye movements. *Curr Opin Neurobiol* 21: 623–628, 2011. doi:10.1016/j.conb.2011.05.023.
80. **Acerbi L, Ma WJ.** Practical Bayesian optimization for model fitting with Bayesian adaptive direct search. *Adv Neural Inf Process Syst* 30: 1837–1847, 2017.
81. **Gellman RS, Carl JR.** Motion processing for saccadic eye movements in humans. *Exp Brain Res* 84: 660–667, 1991. doi:10.1007/BF00230979.
82. **Schreiber C, Missal M, Lefèvre P.** Asynchrony between position and motion signals in the saccadic system. *J Neurophysiol* 95: 960–969, 2006. doi:10.1152/jn.00315.2005.
83. **Groh JM, Born RT, Newsome WT.** How is a sensory map read out? Effects of microstimulation in visual area MT on saccades and smooth pursuit eye movements. *J Neurosci* 17: 4312–4330, 1997. doi:10.1523/JNEUROSCI.17-11-04312.1997.
84. **Darlington TR, Tokiyama S, Lisberger SG.** Control of the strength of visual-motor transmission as the mechanism of rapid adaptation of priors for Bayesian inference in smooth pursuit eye movements. *J Neurophysiol* 118: 1173–1189, 2017. doi:10.1152/jn.00282.2017.
85. **Dash S, Thier P.** Smooth pursuit adaptation (SPA) exhibits features useful to compensate changes in the properties of the smooth pursuit eye movement system due to usage. *Front Syst Neurosci* 7: 67, 2013. doi:10.3389/fnsys.2013.00067.
86. **Ono S, Kizuka T.** Effects of visual error timing on smooth pursuit gain adaptation in humans. *J Mot Behav* 49: 229–234, 2017. doi:10.1080/00222895.2016.1169981.
87. **Chen J, Valsecchi M, Gegenfurtner KR.** Attention is allocated closely ahead of the target during smooth pursuit eye movements: evidence from EEG frequency tagging. *Neuropsychologia* 102: 206–216, 2017. doi:10.1016/j.neuropsychologia.2017.06.024.
88. **Khan AZ, Lefèvre P, Heinen SJ, Blohm G.** The default allocation of attention is broadly ahead of smooth pursuit. *J Vis* 10: 7, 2010. doi:10.1167/10.13.7.
89. **Poletti M, Rucci M, Carrasco M.** Selective attention within the foveola. *Nat Neurosci* 20: 1413–1417, 2017. doi:10.1038/nn.4622.
90. **Kowler E, Aitkin CD, Ross NM, Santos EM, Zhao M.** Davida Teller Award Lecture 2013: The importance of prediction and anticipation in the control of smooth pursuit eye movements. *J Vis* 14: 10, 2014. doi:10.1167/14.5.10.
91. **Zhao M, Gersch TM, Schnitzer BS, Doshier BA, Kowler E.** Eye movements and attention: The role of pre-saccadic shifts of attention in perception, memory and the control of saccades. *Vision Res* 74: 40–60, 2012. doi:10.1016/j.visres.2012.06.017.
92. **Lo C-C, Wang X-J.** Cortico-basal ganglia circuit mechanism for a decision threshold in reaction time tasks. *Nat Neurosci* 9: 956–963, 2006. doi:10.1038/nn1722.
93. **Simen P.** Evidence accumulator or decision threshold which cortical mechanism are we observing? *Front Psychol* 3: 1–14, 2012. doi:10.3389/fpsyg.2012.00183.
94. **Becker W, Jürgens R.** An analysis of the saccadic system by means of double step stimuli. *Vision Res* 19: 967–983, 1979. doi:10.1016/0042-6989(79)90222-0.
95. **Van Gisbergen JAM, van Opstal AJ, Roebroek JGH.** Stimulus-induced midflight modification of saccade trajectories. In: *Eye Movements: From Physiology to Cognition*, edited by O'Regan JK, Levy-Schoen A. Amsterdam: Elsevier, 1987. doi:10.1016/b978-0-444-70113-8.50007-2.
96. **Montagnini A, Chelazzi L.** Dynamic interaction between “go” and “stop” signals in the saccadic eye movement system: new evidence against the functional independence of the underlying neural mechanisms. *Vision Res* 49: 1316–1328, 2009. doi:10.1016/j.visres.2008.07.018.
97. **McPeck RM, Han JH, Keller EL.** Competition between saccade goals in the superior colliculus produces saccade curvature. *J Neurophysiol* 89: 2577–2590, 2003. doi:10.1152/jn.00657.2002.
98. **Port NL, Wurtz RH.** Sequential activity of simultaneously recorded neurons in the superior colliculus during curved saccades. *J Neurophysiol* 90: 1887–1903, 2003. doi:10.1152/jn.01151.2002.
99. **Ramakrishnan A, Sureshbabu R, Murthy A.** Understanding how the brain changes its mind: microstimulation in the macaque frontal eye field reveals how saccade plans are changed. *J Neurosci* 32: 4457–4472, 2012. doi:10.1523/JNEUROSCI.3668-11.2012.
100. **Grimaldi P, Lau H, Basso MA.** There are things that we know that we know, and there are things that we do not know we do not know: confidence in decision-making. *Neurosci Biobehav Rev* 55: 88–97, 2015. doi:10.1016/j.neubiorev.2015.04.006.
101. **Kepecs A, Mainen ZF.** A computational framework for the study of confidence in humans and animals. *Philos Trans R Soc Lond B Biol Sci* 367: 1322–1337, 2012. doi:10.1098/rstb.2012.0037.
102. **Meyniel F, Sigman M, Mainen ZF.** Confidence as Bayesian probability: from neural origins to behavior. *Neuron* 88: 78–92, 2015. doi:10.1016/j.neuron.2015.09.039.
103. **Dotan D, Meyniel F, Dehaene S.** On-line confidence monitoring during decision making. *Cognition* 171: 112–121, 2018 [Erratum in *Cognition* 171: 112–121, 2018]. doi:10.1016/j.cognition.2017.11.001.
104. **De Gardelle V, Le Corre F, Mamassian P.** Confidence as a common currency between vision and audition. *PLoS One* 11: e0147901, 2016. doi:10.1371/journal.pone.0147901.
105. **van den Berg R, Zylberberg A, Kiani R, Shadlen MN, Wolpert DM.** Confidence is the bridge between multi-stage decisions. *Curr Biol* 26: 3157–3168, 2016. doi:10.1016/j.cub.2016.10.021.
106. **Takahashi M, Sugiuchi Y, Shinoda Y.** Topographic organization of excitatory and inhibitory commissural connections in the superior colliculi and their functional roles in saccade generation. *J Neurophysiol* 104: 3146–3167, 2010. doi:10.1152/jn.00554.2010.
107. **Goffart L, Hafed ZM, Krauzlis RJ.** Visual fixation as equilibrium: evidence from superior colliculus inactivation. *J Neurosci* 32: 10627–10636, 2012. doi:10.1523/JNEUROSCI.0696-12.2012.

108. **Sugiuchi Y, Izawa Y, Takahashi M, Na J, Shinoda Y.** Controversy on "fixation zone" of the superior colliculus. *Neuro-Ophthalmology* 31: 147–155, 2007. doi:10.1080/01658100701647688.
109. **Hafed ZM, Goffart L, Krauzlis RJ.** A neural mechanism for microsaccade generation in the primate superior colliculus. *Science* 323: 940–943, 2009. doi:10.1126/science.1166112.
110. **Hafed ZM, Krauzlis RJ.** Similarity of superior colliculus involvement in microsaccade and saccade generation. *J Neurophysiol* 107: 1904–1916, 2012. doi:10.1152/jn.01125.2011.
111. **De Maesschalck R, Jouan-Rimbaud D, Massart DL.** The Mahalanobis distance. *Chemom Intell Lab Syst* 50: 1–18, 2000. doi:10.1016/S0169-7439(99)00047-7.
112. **Mitchell AFS, Krzanowski WJ.** The Mahalanobis distance and elliptic distributions. *Biometrika* 72: 464–467, 1985. doi:10.1093/biomet/72.2.464.
113. **Newsome WT, Wurtz RH, Dürsteler MR, Mikami A.** Deficits in visual motion processing following ibotenic acid lesions of the middle temporal visual area of the macaque monkey. *J Neurosci* 5: 825–840, 1985. doi:10.1523/JNEUROSCI.05-03-00825.1985.
114. **Keller EL, Gandhi NJ, Weir PT.** Discharge of superior collicular neurons during saccades made to moving targets. *J Neurophysiol* 76: 3573–3577, 1996. doi:10.1152/jn.1996.76.5.3573.
115. **Krauzlis RJ, Basso MA, Wurtz RH.** Discharge properties of neurons in the rostral superior colliculus of the monkey during smooth-pursuit eye movements. *J Neurophysiol* 84: 876–891, 2000. doi:10.1152/jn.2000.84.2.876.
116. **Basso MA, Krauzlis RJ, Wurtz RH.** Activation and inactivation of rostral superior colliculus neurons during smooth-pursuit eye movements in monkeys. *J Neurophysiol* 84: 892–908, 2000. doi:10.1152/jn.2000.84.2.892.
117. **Hafed ZM, Goffart L, Krauzlis RJ.** Superior colliculus inactivation causes stable offsets in eye position during tracking. *J Neurosci* 28: 8124–8137, 2008. doi:10.1523/JNEUROSCI.1317-08.2008.
118. **Lynch JC, Hoover JE, Strick PL.** Input to the primate frontal eye field from the substantia nigra, superior colliculus, and dentate nucleus demonstrated by transneuronal transport. *Exp Brain Res* 100: 181–186, 1994. doi:10.1007/BF00227293.
119. **Ungerleider LG, Desimone R.** Cortical connections of visual area MT in the macaque. *J Comp Neurol* 248: 190–222, 1986. doi:10.1002/cne.902480204.
120. **Coppe S, Orban de Xivry J-J, Yüksel D, Ivanou A, Lefèvre P.** Dramatic impairment of prediction due to frontal lobe degeneration. *J Neurophysiol* 108: 2957–2966, 2012. doi:10.1152/jn.00582.2012.
121. **Crapse TB, Sommer MA.** The frontal eye field as a prediction map. *Prog Brain Res* 171: 383–390, 2008. doi:10.1016/S0079-6123(08)00656-0.
122. **Bakst L, Fleuriot J, Mustari MJ.** Temporal dynamics of retinal and extraretinal signals in the FEFsem during smooth pursuit eye movements. *J Neurophysiol* 117: 1987–2003, 2017. doi:10.1152/jn.00786.2016.
123. **Berman RA, Colby CL, Genovese CR, Voyvodic JT, Luna B, Thulborn KR, Sweeney JA.** Cortical networks subserving pursuit and saccadic eye movements in humans: an fMRI study. *Hum Brain Mapp* 8: 209–225, 1999. doi:10.1002/(SICI)1097-0193(1999)8:4<209::AID-HBM5>3.0.CO;2-0.
124. **Huk AC, Shadlen MN.** Neural activity in macaque parietal cortex reflects temporal integration of visual motion signals during perceptual decision making. *J Neurosci* 25: 10420–10436, 2005. doi:10.1523/JNEUROSCI.4684-04.2005.
125. **Konen CS, Kastner S.** Representation of eye movements and stimulus motion in topographically organized areas of human posterior parietal cortex. *J Neurosci* 28: 8361–8375, 2008. doi:10.1523/JNEUROSCI.1930-08.2008.
126. **Yates JL, Park IM, Katz LN, Pillow JW, Huk AC.** Functional dissection of signal and noise in MT and LIP during decision-making. *Nat Neurosci* 20: 1285–1292, 2017. doi:10.1038/nn.4611.
127. **Hanes DP, Schall JD.** Neural control of voluntary movement initiation. *Science* 274: 427–430, 1996. doi:10.1126/science.274.5286.427.
128. **Kiani R, Shadlen MN.** Representation of confidence associated with a decision by neurons in the parietal cortex. *Science* 324: 759–764, 2009. doi:10.1126/science.1169405.
129. **Cui D-MM, Yan Y-JJ, Lynch JC.** The pursuit subregion of the frontal eye field projects to the caudate nucleus in monkeys. *J Neurophysiol* 89: 2678–2684, 2003. doi:10.1152/jn.00501.2002.
130. **Ma WJ.** Signal detection theory, uncertainty, and Poisson-like population codes. *Vision Res* 50: 2308–2319, 2010. doi:10.1016/j.visres.2010.08.035.
131. **Jazayeri M, Movshon A.** Optimal representation of sensory information by neural populations. *Nat Neurosci* 9: 690–696, 2006. doi:10.1038/nn1691.
132. **Ma WJ, Beck JM, Latham PE, Pouget A.** Bayesian inference with probabilistic population codes. *Nat Neurosci* 9: 1432–1438, 2006. doi:10.1038/nn1790.
133. **Orbán G, Berkes P, Fiser J, Lengyel M.** Neural variability and sampling-based probabilistic representations in the visual cortex. *Neuron* 92: 530–543, 2016. doi:10.1016/j.neuron.2016.09.038.
134. **Dash S, Yan X, Wang H, Crawford JD.** Continuous updating of visuospatial memory in superior colliculus during slow eye movements. *Curr Biol* 25: 267–274, 2015. doi:10.1016/j.cub.2014.11.064.
135. **Goffart L, Cecala AL, Gandhi NJ.** The superior colliculus and the steering of saccades toward a moving visual target. *J Neurophysiol* 118: 2890–2901, 2017. doi:10.1152/jn.00506.2017.
136. **Nachmani O, Coutinho J, Khan AZ, Lefèvre P, Blohm G.** Predicted position error triggers catch-up saccades during sustained smooth pursuit. *eNeuro* 7: ENEURO.0196-18.2019, 2019. doi:10.1523/ENEURO.0196-18.2019.
137. **Heinen SJ, Potapchuk E, Watamaniuk SNJ.** A foveal target increases catch-up saccade frequency during smooth pursuit. *J Neurophysiol* 115: 1220–1227, 2015. doi:10.1152/jn.00774.2015.
138. **Munoz DP, Wurtz RH.** Fixation cells in monkey superior colliculus. I. Characteristics of cell discharge. *J Neurophysiol* 70: 559–575, 1993. doi:10.1152/jn.1993.70.2.559.
139. **Brenner E, Smeets JB.** How people achieve their amazing temporal precision in interception. *J Vis* 15: 1–21, 2015. doi:10.1167/15.3.8.doi.
140. **Brenner E, Smeets JB.** Sources of variability in interceptive movements. *Exp Brain Res* 195: 117–133, 2009. doi:10.1007/s00221-009-1757-x.
141. **Soechting JF, Juveli JZ, Rao HM.** Models for the extrapolation of target motion for manual interception. *J Neurophysiol* 102: 1491–1502, 2009. doi:10.1152/jn.00398.2009.
142. **Soechting JF, Flanders M.** Extrapolation of visual motion for manual interception. *J Neurophysiol* 99: 2956–2967, 2008. doi:10.1152/jn.90308.2008.
143. **Diaz GJ, Cooper J, Rothkopf CA, Hayhoe MM.** Saccades to future ball location reveal memory-based prediction in a virtual-reality interception task. *J Vis* 13: 20, 2013. doi:10.1167/13.1.20.
144. **Hayhoe MM, Shrivastava A, Mruczek R, Pelz JB.** Visual memory and motor planning in a natural task. *J Vis* 3: 6, 2003. doi:10.1167/3.1.6.
145. **Fooken J, Yeo S-H, Pai DK, Spering M.** Eye movement accuracy determines natural interception strategies. *J Vis* 16: 1–15, 2016. doi:10.1167/16.14.1.
146. **Goettker A, Brenner E, Gegenfurtner KR, de la Malla C.** Corrective saccades influence velocity judgments and interception. *Sci Rep* 9: 5395, 2019. doi:10.1038/s41598-019-41857-z.
147. **Mongeau JM, Frye MA.** *Drosophila* spatiotemporally integrates visual signals to control saccades. *Curr Biol* 27: 2901–2914.e2, 2017. doi:10.1016/j.cub.2017.08.035.
148. **Mongeau J-M, Cheng KY, Aptekar J, Frye MA.** Visuomotor strategies for object approach and aversion in *Drosophila melanogaster*. *J Exp Biol* 222: jeb.193730, 2018. doi:10.1242/jeb.193730.
149. **Bianco IH, Kampff AR, Engert F.** Prey capture behavior evoked by simple visual stimuli in larval zebrafish. *Front Syst Neurosci* 5: 101, 2011. doi:10.3389/fnsys.2011.00101.
150. **Semmelhack JL, Donovan JC, Thiele TR, Kuehn E, Laurell E, Baier H.** A dedicated visual pathway for prey detection in larval zebrafish. *eLife* 3: 4878, 2014. doi:10.7554/eLife.04878.
151. **Bianco IH, Engert F.** Visuomotor transformations underlying hunting behavior in zebrafish. *Curr Biol* 25: 831–846, 2015. doi:10.1016/j.cub.2015.01.042.
152. **Dunn TW, Gebhardt C, Naumann EA, Riegler C, Ahrens MB, Engert F, Del Bene F.** Neural circuits underlying visually evoked escapes in larval zebrafish. *Neuron* 89: 613–628, 2016. doi:10.1016/j.neuron.2015.12.021.

153. **Fajardo O, Zhu P, Friedrich RW.** Control of a specific motor program by a small brain area in zebrafish. *Front Neural Circuits* 7: 67, 2013. doi:10.3389/fncir.2013.00067.
154. **Romano SA, Pietri T, Pérez-Schuster V, Jouary A, Haudrechy M, Sumbre G.** Spontaneous neuronal network dynamics reveal circuit's functional adaptations for behavior. *Neuron* 85: 1070–1085, 2015. doi:10.1016/j.neuron.2015.01.027.
155. **Marachlian E, Avitan L, Goodhill GJ, Sumbre G.** Principles of functional circuit connectivity: Insights from spontaneous activity in the zebrafish optic tectum. *Front Neural Circuits* 12: 1–8, 2018. doi:10.3389/fncir.2018.00001.
156. **Clemens J, Murthy M.** The use of computational modeling to link sensory processing with behavior in drosophila. In: *Decoding Neural Circuit Structure and Function*, edited by Çelik A, Wernet M. Cham, Switzerland: Springer International Publishing, 2017, pp. 241–260. doi:10.1007/978-3-319-57363-2\_9.
157. **Orger MB.** The cellular organization of zebrafish visuomotor circuits. *Curr Biol* 26: R377–R385, 2016. doi:10.1016/j.cub.2016.03.054.
158. **Stowers JR, Hofbauer M, Bastien R, Griessner J, Higgins P, Farooqui S, Fischer RM, Nowikovsky K, Haubensak W, Couzin ID, Tessmar-Raible K, Straw AD.** Virtual reality for freely moving animals. *Nat Methods* 14: 995–1002, 2017. doi:10.1038/nmeth.4399.